

AD-A168 481

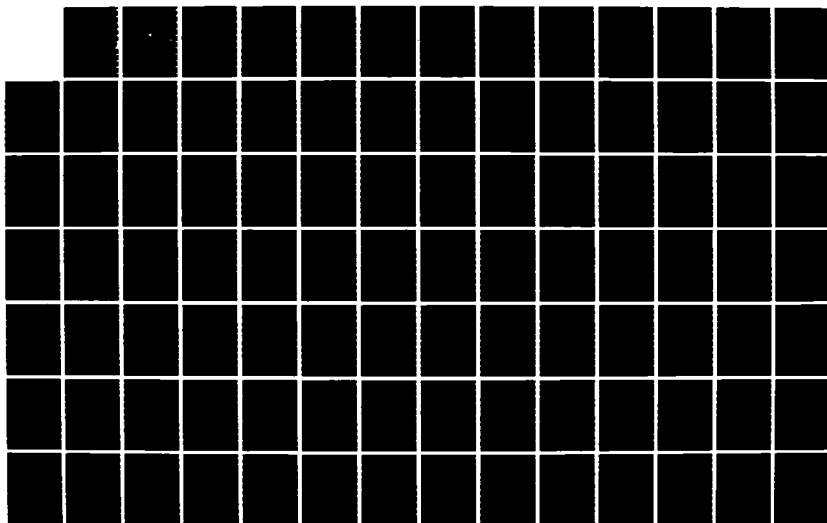
CONTRIBUTION TO THE ANALYSIS OF HIGH-LIFT AIRFOIL
AERODYNAMICS(U) NAVAL POSTGRADUATE SCHOOL MONTEREY CA
H W LEE MAR 86

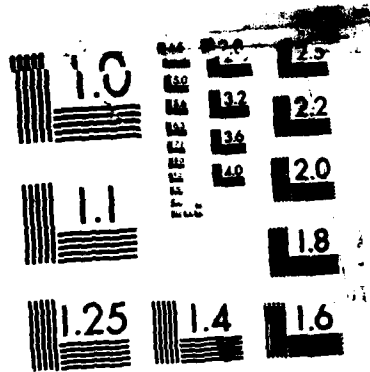
1/2

UNCLASSIFIED

F/G 20/4

NL





MICROCOPY RESOLUTION TEST CHART
NATIONAL BUREAU OF STANDARDS - 1963-A

2

NAVAL POSTGRADUATE SCHOOL

Monterey, California

AD-A168 401



SDTIC
ELECTE
JUN 10 1986
S E D

THESIS

CONTRIBUTION TO THE ANALYSIS OF
HIGH-LIFT AIRFOIL AERODYNAMICS

by

Hee Woo Lee

March 1986

Thesis Advisor:

M.F. Platzer

Approved for public release; distribution is unlimited.

DTIC FILE COPY

86 6 10 115

UNCLASSIFIED

SECURITY CLASSIFICATION OF THIS PAGE

REPORT DOCUMENTATION PAGE

1a. REPORT SECURITY CLASSIFICATION Unclassified			1b. RESTRICTIVE MARKINGS	
2a. SECURITY CLASSIFICATION AUTHORITY			3. DISTRIBUTION/AVAILABILITY OF REPORT Approved for public release; distribution is unlimited	
2b. DECLASSIFICATION/DOWNGRADING SCHEDULE			5. MONITORING ORGANIZATION REPORT NUMBER(S)	
4. PERFORMING ORGANIZATION REPORT NUMBER(S)				
6a. NAME OF PERFORMING ORGANIZATION Naval Postgraduate School	6b. OFFICE SYMBOL (If applicable) Code 67	7a. NAME OF MONITORING ORGANIZATION Naval Postgraduate School		
6c. ADDRESS (City, State, and ZIP Code) Monterey, California 93943-5100		7b. ADDRESS (City, State, and ZIP Code) Monterey, California 93943-5100		
8a. NAME OF FUNDING/SPONSORING ORGANIZATION	8b. OFFICE SYMBOL (If applicable)	9. PROCUREMENT INSTRUMENT IDENTIFICATION NUMBER		
8c. ADDRESS (City, State, and ZIP Code)		10. SOURCE OF FUNDING NUMBERS		
		PROGRAM ELEMENT NO	PROJECT NO	TASK NO
		WORK UNIT ACCESSION NO		
11. TITLE (Include Security Classification) CONTRIBUTION TO THE ANALYSIS OF HIGH-LIFT AIRFOIL AERODYNAMICS				
12. PERSONAL AUTHOR(S) Lee, Hee W.				
13a. TYPE OF REPORT Master's Thesis	13b. TIME COVERED FROM TO	14. DATE OF REPORT (Year, Month, Day) 1986, March	15. PAGE COUNT 102	
16. SUPPLEMENTARY NOTATION				
17. COSATI CODES			18. SUBJECT TERMS (Continue on reverse if necessary and identify by block number)	
FIELD	GROUP	SUB-GROUP		
			Computational Analysis of Inviscid, Viscous, and Interaction Schemes	
19. ABSTRACT (Continue on reverse if necessary and identify by block number)				
<p>This thesis treats the problem of incompressible two-dimensional steady flow past airfoils or airfoil combinations at large angles of attack. A panel method was developed to compute the inviscid flow over two cylinders, airfoil-flap combinations and airfoils in ground effect. In addition, Cebeci's viscous/inviscid interaction method was applied to several airfoils and compared with available experimental data. The agreement is generally quite encouraging.</p>				
20. DISTRIBUTION/AVAILABILITY OF ABSTRACT <input checked="" type="checkbox"/> UNCLASSIFIED/UNLIMITED <input type="checkbox"/> SAME AS RPT <input type="checkbox"/> DTIC USERS			21. ABSTRACT SECURITY CLASSIFICATION Unclassified	
22a. NAME OF RESPONSIBLE INDIVIDUAL Prof. Max. F. Platzer			22b. TELEPHONE (Include Area Code) (408) 646-2944	22c. OFFICE SYMBOL Code 67P1

Approved for public release; distribution is unlimited.

Contribution to the Analysis of
High-Lift Airfoil Aerodynamics

by

Hee Woo Lee
Captain, Korea Air Force
B.S., Korea Air Force Academy, 1979

Submitted in partial fulfillment of the
requirements for the degree of

AERONAUTICAL ENGINEER

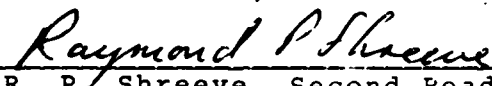
from the
NAVAL POSTGRADUATE SCHOOL
March 1986

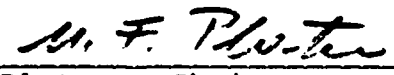
Author:



Hee Woo Lee

Approved by:


M. F. Platzter, Thesis Advisor


R. P. Shreeve, Second Reader


M. F. Platzter, Chairman
Department of Aeronautics


John N. Dyer, Dean of Science and Engineering

ABSTRACT

This thesis treats the problem of incompressible two-dimensional steady flow past airfoils or airfoil combinations at large angles of attack. A panel method was developed to compute the inviscid flow over two cylinders, airfoil-flap combinations and airfoils in ground effect. In addition, Cebeci's viscous/inviscid interaction method was applied to several airfoils and compared with available experimental data. The agreement is generally quite encouraging.

Accession For	
NTIS GRA&I	<input checked="checked" type="checkbox"/>
DTIC TAB	<input type="checkbox"/>
Unannounced	<input type="checkbox"/>
Justification	
By _____	
Distribution /	
Avail	Codes
Dist	

A-1



TABLE OF CONTENTS

I.	INTRODUCTION -----	12
II.	BASIC EQUATIONS -----	14
	A. INTRODUCTION -----	14
	B. DERIVATION OF GENERAL EQUATIONS -----	15
	1. Continuity Equation -----	15
	2. Navier-Stokes Equations -----	18
	C. INVISCID FLOW EQUATION -----	22
	1. Velocity Potential -----	23
	2. Laplace Equation -----	23
	D. THIN SHEAR LAYER EQUATIONS -----	24
	E. TURBULENT FLOW -----	27
III.	PANEL METHOD -----	29
	A. INTRODUCTION -----	29
	B. NONLIFTING FLOW PAST A BODY -----	30
	C. CIRCULATORY FLOW -----	40
	D. SYNTHESIZING A COMBINED FLOW -----	43
	E. EXAMPLES -----	47
	F. I/O--DESCRIPTION AND LISTING OF THE PROGRAM "PANEL" -----	55
IV.	BOX METHOD -----	67
	A. INTRODUCTION -----	67
	B. FALKNER-SKAN TRANSFORMATION -----	67
	C. NUMERICAL FORMULATION (BOX METHOD) -----	69
	D. BLOCK ELIMINATION METHOD -----	73

V.	INTERACTION METHOD -----	79
A.	INTRODUCTION -----	79
B.	FOUNDATION OF THE INTERACTION SCHEMES -----	81
1.	Direct Interaction Scheme -----	81
2.	Inverse Interaction Scheme -----	83
3.	Semi-Inverse Interaction Scheme -----	83
4.	Simultaneous Interaction Scheme -----	84
C.	CONSIDERATION OF BOUNDARY LAYER TRANSI- TION AND OF TURBULENCE FLOW MODELLING -----	87
1.	Transition -----	87
2.	Turbulence Model -----	88
D.	EXAMPLES -----	88
1.	Demonstration of the Program Capabilities -----	89
2.	Comparison with Experimental Results --	93
VI.	SUMMARY AND RECOMMENDATIONS -----	98
	LIST OF REFERENCES -----	99
	INITIAL DISTRIBUTION LIST -----	101

LIST OF TABLES

2.1	CLASSIFICATION OF PDE'S -----	14
-----	-------------------------------	----

LIST OF FIGURES

2.1	Control Volume for 2-D -----	16
2.2	Forces Acting on the Fluid -----	19
3.1	Boundary Condition at One Inclined Panel -----	31
3.2	Designations for Calculation -----	33
3.3	Single Airfoil: Superposition of Nonlifting and Circulatory Flow, Controlled by Kutta Condition -----	44
3.4	Two Element Airfoil: Superposition of Nonlifting and Circulatory Flows -----	46
3.5	Arrangement of Panels on a Circular Cylinder ---	47
3.6	Pressure Coefficient on a Circular Cylinder Obtained by Using Eight Source Panels (Marked by 0) in Comparison with the Exact Solution ----	48
3.7	(a) Arrangement of Panels on Two Cylinders Side by Side (b) Calculated Velocity Distribution on One of Two Identical Circular Cylinders Whose Centers Are One and a Quarter Diameters Apart -----	50
3.8	Streamlines of Flow Past Two Identical Cylinders Whose Centers Are One and a Quarter Diameters Apart -----	51
3.9	Pressure Distributions on a Single and an Airfoil with a Slotted Flap -----	52
3.10	Airfoil in Ground Effect ($\alpha = 5$ degrees) -----	53
3.11	Pressure Distributions on a Single NACA 4412 and a NACA 4412 in Ground Effect ($h/c = 0.2$, $\alpha = 5^\circ$) -----	54
3.12	The Lift on a NACA 4412 Near the Ground -----	54
4.1	Transformed Coordinates of Upper Surface Air- foil and Net Rectangle for Difference Approximations -----	69

5.1	Global Organization of Interaction Methods -----	82
5.2	Blowing Velocity Concept -----	85
5.3	Velocity Profiles on the Surface and Wake of FX 63-137 Airfoil ($\alpha = 10^\circ$, $Re = 5 \times 10^6$) ----	90
5.4	(a) Lift, (b) Drag, (c) Transition Points Calculations (FX 63-137 Airfoil, $Re = 5 \times 10^6$) --	91
5.5	Skin Friction Coefficient, Displacement Thickness and Shape Parameter for FX 63-137 ----	92
5.6	Comparison of Pressure Distributions (NACA 4412 Airfoil, $\alpha = 12.15^\circ$) -----	94
5.7	C_ℓ and C_d Curves for (a) FX 63-137, $Re = 199487$ (b) GA-1, $Re = 1900000$, (c) FX 63-137, $Re = 280000$ -----	95
5.8	Transition and Separation Positions for NACA 64 ₃ -418, $Re = 0.93 \times 10^6$ -----	97

TABLE OF SYMBOLS

u	velocity component in x direction
v	velocity component in y direction
ρ	density
μ	viscosity
ν	kinematic viscosity
P	local static pressure
m	mass
σ	stress
ϕ	velocity potential
$O()$	order of magnitude
V_{∞}	free stream velocity
λ	source strength
θ	angle between flow direction and x-axis
β	angle between normal to the flow direction and x-axis
α	angle of attack
Φ	total velocity potential
C_p	pressure coefficient
Γ	circulation strength
h	height
c	chord length
U_e	external velocity
ψ	stream function
ν_t	kinematic viscosity due to turbulent flow

δ^* displacement thickness
 ω relaxation parameter
 C_f skin friction coefficient
 C_l lift coefficient
 C_d drag coefficient

ACKNOWLEDGMENTS

I would like to express my thanks to Professor Platzner for his tireless assistance in making this thesis a worthwhile and enjoyable learning experience. Thanks are also due Andreas Krainer and Dennis Mar. Furthermore, I would like to thank Dr. Cebeci and Dr. Giesing for the use of their programs and their assistance.

I. INTRODUCTION

Two important parameters of interest in the field of aerodynamics of airfoils are lift and drag. These can be evaluated either experimentally or theoretically. The desire for computational methods to aid the design process is promoted by the need to reduce the number and cost of wind tunnel tests.

This thesis treats the problem of incompressible, two-dimensional steady flow about airfoils or airfoil combinations at large angles of attack. Such flows exhibit strong viscous flow effects including regions of flow separation. Therefore methods are required which can account for these effects.

Currently there exist two main methods, namely the direct computation of viscous flows by means of the Navier-Stokes equations or the so-called viscous/inviscid interaction method. The former approach is more straightforward but also much more expensive and time-consuming. Therefore, the latter approach is to be preferred if it can be shown that it produces good agreement with the available experimental results.

It is the purpose of this thesis to contribute to the evaluation of the viscous/inviscid interaction method. To this end, the viscous/inviscid computer codes developed by Cebeci and collaborators at the Douglas Aircraft Company were obtained and applied to several airfoils.

In addition, a separate panel method was formulated and programmed in order to obtain the inviscid flow over airfoil combinations.



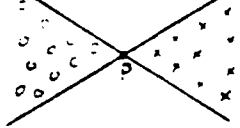
The basic equations are formulated in Chapter II. Chapter III addresses the problem of inviscid flow calculations using the panel method. In Chapter IV the solution of the boundary layer equations by means of the Cebeci-Keller box method is explained. Finally, Chapter V describes the viscous/inviscid interaction problem and presents results of computations.

II. BASIC EQUATIONS

A. INTRODUCTION

In this chapter, the basic equations of fluid flow are derived. We find that the resulting equations are PDE's whose exact solutions exist only in very few cases. The PDE's are classified, "parabolic," "hyperbolic," "elliptic" depending on the geometry of their domains of dependence and regions of influence, and the solution procedures are different according to the type of equation. Table 2-1 gives a brief classification of these equations.

TABLE 2-1
CLASSIFICATION OF PDE'S

	Elliptic	Parabolic	Hyperbolic
			
Physical Meaning	Upstream Influence	No Upstream Influence	No Upstream Influence
Example Equations	<ul style="list-style-type: none"> • Laplace • Steady Navier-Stokes 	<ul style="list-style-type: none"> • Thin Shear Layer 	<ul style="list-style-type: none"> • Supersonic Flow

: P is perturbation point



is domain on which solution at P depends



is region of influence of a perturbation at P

For example, the Laplace equation is elliptic. Its solution would have to be repeated for many iterations so that the upstream influence can be gradually propagated (panel method in Chapter III), but the thin shear layer equations are parabolic. Their numerical solution can be obtained by marching in the downstream direction only (Box method in Chapter IV).

B. DERIVATION OF GENERAL EQUATIONS

The continuity equation and the Navier-Stokes equations are basic for an aerodynamic analysis. We start with the basic physical concepts and derive the general equations for 2-D, unsteady, compressible, viscous flow.

1. Continuity Equation

One of the basic laws of "Newtonian mechanics" states that mass can neither be created nor destroyed. Therefore, for a fixed control volume (see Figure 2.1), the principle of mass conservation can be stated that the net mass flow rate into and out of the control volume equals the time rate of change of mass within the control volume.

If the central point 'P' has representative fluid properties (velocity, density, pressure, etc.), then properties at other locations can be obtained by Taylor series expansions. Therefore the x-component of the velocity at the center of the positive x-face (right-hand face) is

$$u + \frac{\partial u}{\partial x} \left(\frac{dx}{2} \right) + \frac{\partial^2 u}{\partial x^2} \left(\frac{dx}{2} \right)^2 \frac{1}{2!} + \dots \quad (2.1)$$

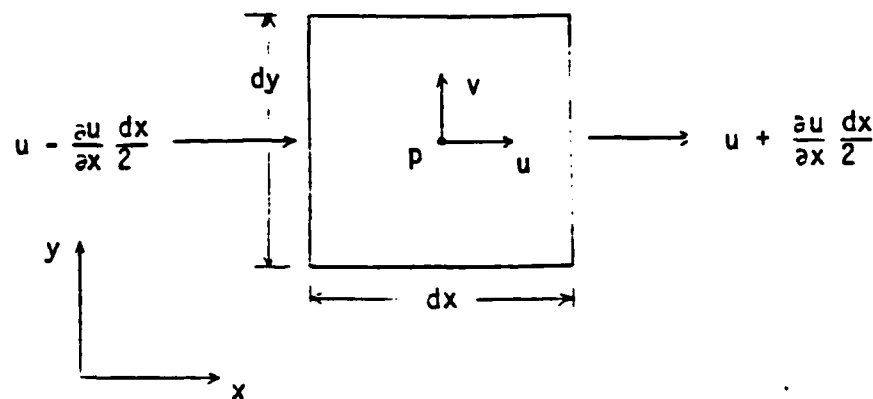


Figure 2.1. Control Volume for 2-D

As dx goes to zero, all higher order terms will be dropped, so that only the first two terms will be considered. Similarly, the density at the center of the positive x -face is

$$\rho + \frac{\partial \rho}{\partial x} \frac{dx}{2} + \dots \quad (2.2)$$

Then the mass flow rate out of the positive x -face is

$$\begin{aligned} \text{Mass Flow Rate Out} &= (\text{Density}) (\text{Velocity}) (\text{Area}) \\ &= \left(\rho + \frac{\partial \rho}{\partial x} \frac{dx}{2} + \dots \right) \left(u + \frac{\partial u}{\partial x} \frac{dx}{2} + \dots \right) dy \\ &= \left[\rho u + \frac{\partial}{\partial x} (\rho u) \frac{dx}{2} \right] dy \end{aligned} \quad (2.3)$$

By the same procedure the mass flow rate into the control volume through the negative x -face (left-hand side) is

$$\text{Mass Flow Rate In} = \left[\rho u - \frac{\partial}{\partial x}(\rho u) \frac{dx}{2} \right] dy \quad (2.4)$$

From Eqs. (2.3) and (2.4), we get the net mass flow rate through the control volume in the x-direction.

$$\begin{aligned} \text{Net Mass Flow Rate} &= \left[\rho u - \frac{\partial}{\partial x}(\rho u) \frac{dx}{2} \right] dy - \left[\rho u + \frac{\partial}{\partial x}(\rho u) \frac{dx}{2} \right] dy \\ &= - \frac{\partial}{\partial x}(\rho u) dx dy \end{aligned} \quad (2.5)$$

In a similar manner, the net mass flow rate in the y-direction is

$$- \frac{\partial}{\partial y}(\rho v) dx dy \quad (2.6)$$

The total mass flow rate through the control volume is obtained by summing Eqs. (2.5) and (2.6).

$$\text{Total Net Mass Flow Rate} = - \left[\frac{\partial}{\partial x}(\rho u) + \frac{\partial}{\partial y}(\rho v) \right] dx dy \quad (2.7)$$

Next, we consider the time rate of change of mass within the control volume.

$$\begin{aligned} \text{Time Rate of Change of Mass} &= \frac{\partial}{\partial t}(\rho dx dy) \\ &= \frac{\partial \rho}{\partial t} dx dy \end{aligned} \quad (2.8)$$

Now we combine Eqs. (2.7) and (2.8) using the concept of conservation of mass. Then

$$-\left[\frac{\partial}{\partial x}(\rho u) + \frac{\partial}{\partial y}(\rho v)\right]dx dy = \frac{\partial \rho}{\partial t} dx dy \quad (2.9)$$

Therefore we obtain the general form of the continuity equation for two-dimensional flow as

$$\frac{\partial(\rho u)}{\partial x} + \frac{\partial(\rho v)}{\partial y} + \frac{\partial \rho}{\partial t} = 0 \quad (2.10)$$

For steady or unsteady incompressible flow, Eq. (2.10) reduces to

$$\frac{\partial u}{\partial x} + \frac{\partial v}{\partial y} = 0. \quad (2.10a)$$

2. Navier-Stokes Equations

Newton's second law of motion, when mass is conserved, equivalently states that the rate of change of the momentum of a body equals the sum of the forces applied to that body, or

$$\sum \vec{F} = \frac{d}{dt}(m\vec{V}) \quad (2.11)$$

In considering a small volume element of fluid, there are two types of forces to be considered, namely surface forces which are acting on the surface and body forces which are acting on the fluid inside the elemental volume, such as gravity (see Figure 2.2).

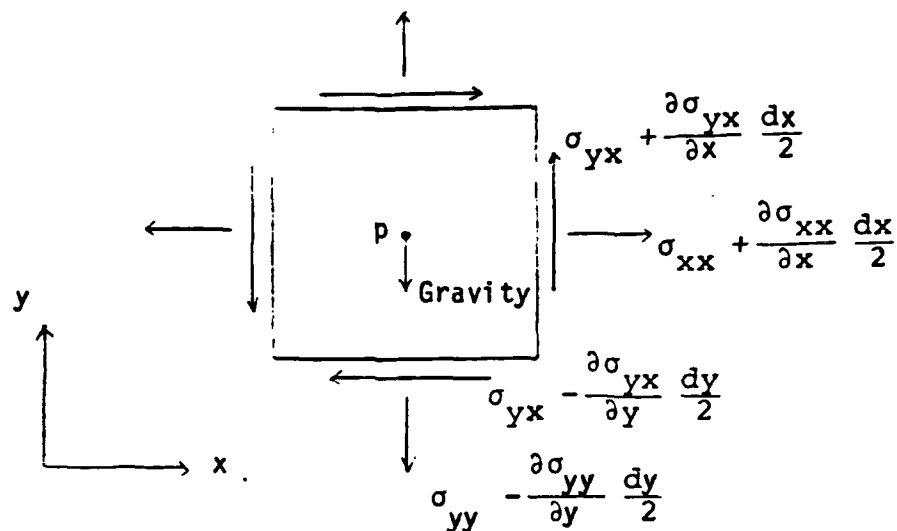


Figure 2.2. Forces Acting on the Fluid

Assuming that the stresses are known at point 'P', we get expressions for the stresses on the fluid element surfaces by Taylor series expansion.

$$\begin{aligned}
 \text{Net force in} & \\
 \text{x-direction due} & \\
 \text{to Normal Stresses} & = \left[\sigma_{xx} + \frac{\partial \sigma_{xx}}{\partial x} \frac{dx}{2} \right] dy - \left[\sigma_{xx} - \frac{\partial \sigma_{xx}}{\partial x} \frac{dx}{2} \right] dy \\
 & = \frac{\partial \sigma_{xx}}{\partial x} dx dy \quad (2.12)
 \end{aligned}$$

$$\begin{aligned}
 \text{Net force in} & \\
 \text{x-direction due} & \\
 \text{to Shear Stresses} & = \left[\sigma_{yx} + \frac{\partial \sigma_{yx}}{\partial y} \frac{dy}{2} \right] dx - \left[\sigma_{yx} - \frac{\partial \sigma_{yx}}{\partial y} \frac{dy}{2} \right] dx \\
 & = \frac{\partial \sigma_{yx}}{\partial y} dx dy \quad (2.13)
 \end{aligned}$$

Therefore the total surface forces in the x-direction are formed by summation of Eqs. (2.12) and (2.13).

$$\int f_x \text{ (surface)} = \left[\frac{\partial \sigma_{xx}}{\partial x} + \frac{\partial \sigma_{yx}}{\partial y} \right] dx dy \quad (2.14)$$

Let \vec{f} (body) be defined as the body force per unit mass with the following components:

$$\vec{f} \text{ (body)} = x \vec{i} + y \vec{j}$$

Thus, the x-component of the body force is

$$\begin{aligned} f_x \text{ (body)} &= m X \\ &= \rho dx dy \cdot 1 \cdot x \end{aligned} \quad (2.15)$$

Adding Eqs. (2.14) and (2.15) provides the total force in the x-direction.

$$\begin{aligned} \int F_x &= f_x \text{ (surface)} \text{ and } f_x \text{ (body)} \\ &= \left[\rho X + \frac{\partial \sigma_{xx}}{\partial x} + \frac{\partial \sigma_{yx}}{\partial y} \right] dx dy \end{aligned} \quad (2.16)$$

Now we consider the rate of change of the momentum of the fluid.

Let us take the x-component only. Then, since the mass is constant,

$$\begin{aligned} \frac{d}{dt} (m\vec{V}) \Big|_x &= m \frac{du}{dt} \\ &= \rho dx dy \left(u \frac{\partial u}{\partial x} + v \frac{\partial u}{\partial y} + \frac{\partial u}{\partial t} \right) \end{aligned} \quad (2.17)$$

because, $u = f[x(t), y(t), t]$, and by chain-rule

$$\begin{aligned}\frac{du}{dt} &= \frac{\partial u}{\partial x} \frac{dx}{dt} + \frac{\partial u}{\partial y} \frac{dy}{dt} + \frac{\partial u}{\partial t} \frac{\partial t}{\partial t} \\ &= u \frac{\partial u}{\partial x} + v \frac{\partial u}{\partial y} + \frac{\partial u}{\partial t}\end{aligned}$$

Substitution of Eqs. (2.16) and (2.17) into the x-component of Eq. (2.11) gives the final equation of motion.

$$\rho X + \frac{\partial \sigma_{xx}}{\partial x} + \frac{\partial \sigma_{yx}}{\partial y} = \rho \left[u \frac{\partial u}{\partial x} + v \frac{\partial u}{\partial y} + \frac{\partial u}{\partial t} \right] \quad (2.18)$$

Now we want to show the stress in terms of the velocity components. In this thesis we will consider only simple "Newtonian" fluids obeying Stokes' law. This means that the 'extra' stress (above hydrostatic pressure) is proportional to the rate of strain. With the definition,

$$\text{Extra Stress} = \text{constant} \times (\text{rate of strain})$$

and introducing $\mu = \text{coefficient of viscosity}$,

$$\sigma_{xx} = -P + 2\mu \left(\frac{\partial u}{\partial x} \right)$$

$$\sigma_{xy} = \mu \left(\frac{\partial u}{\partial y} + \frac{\partial v}{\partial x} \right)$$

where the pressure in an incompressible fluid is seen to be equal to minus one-third the sum of the three normal-stress

components in view of Eq. (2.10a). In two dimensions then,
 $\sigma_{xx} + \sigma_{yy} = -2P$. Eq. (2.18) then becomes, if the body force
 is neglected

$$\frac{\partial u}{\partial t} + u \frac{\partial u}{\partial x} + v \frac{\partial u}{\partial y} = -\frac{1}{\rho} \frac{\partial P}{\partial x} + \frac{1}{\rho} \frac{\partial \sigma_{xx}}{\partial x} + \frac{1}{\rho} \frac{\partial \sigma_{xy}}{\partial y} \quad (2.19)$$

Substitution then produces, for incompressible flow,

$$\frac{\partial u}{\partial t} + u \frac{\partial u}{\partial x} + v \frac{\partial u}{\partial y} = -\frac{1}{\rho} \frac{\partial P}{\partial x} + \nu \left[\frac{\partial^2 u}{\partial x^2} + \frac{\partial^2 u}{\partial y^2} \right] \quad (2.20)$$

where $\nu = \mu/\rho$ = kinematic viscosity, and similarly for the
 y-component

$$\frac{\partial v}{\partial t} + u \frac{\partial v}{\partial x} + v \frac{\partial v}{\partial y} = -\frac{1}{\rho} \frac{\partial P}{\partial y} + \nu \left[\frac{\partial^2 v}{\partial x^2} + \frac{\partial^2 v}{\partial y^2} \right] \quad (2.21)$$

These are the well-known Navier-Stokes equations for two-
 dimensional incompressible viscous flow.

C. INVISCID FLOW EQUATION

All real fluid flows are viscous, but inviscid flow can
 be assumed outside of a thin boundary layer and a narrow wake
 behind the body for large Reynolds numbers. This is the reason
 why the inviscid flow equations are important even though they
 represent an ideal case. If the flow far upstream is uniform
 then it is also irrotational. This allows the introduction of
 the velocity potential.

1. Velocity Potential

The velocity potential ϕ is a function whose gradient represents the fluid velocity. Thus

$$\frac{\partial \phi}{\partial x} = u \quad \frac{\partial \phi}{\partial y} = v \quad (2.22)$$

where

$$\phi = \phi(x, y, t)$$

Therefore, the significance of the velocity potential lies in the fact that one equation for ϕ can be used rather than three equations for the velocity components.

2. Laplace Equation

For steady, incompressible flow, the continuity equation (2.10) becomes

$$\frac{\partial u}{\partial x} + \frac{\partial v}{\partial y} = 0 \quad (2.23)$$

This equation can be written in terms of velocity potential ϕ by substituting Eq. (2.22). Thus

$$\frac{\partial^2 \phi}{\partial x^2} + \frac{\partial^2 \phi}{\partial y^2} = 0 \quad (2.24)$$

This is the well-known Laplace equation (vector form is $\nabla^2 \phi = 0$). It is a linear equation which makes it possible to apply the principle of linear superposition. For instance,

If $\phi_1, \phi_2, \dots, \phi_n$ satisfy $\nabla^2 \phi = 0$, then also $\phi = \phi_1 + \phi_2 + \dots + \phi_n$ satisfies $\nabla^2 \phi = 0$.

Thus the flow resulting from the superposition of incompressible, irrotational flows is also an incompressible and irrotational flow. This superposition principle makes it possible to build up quite complicated flow from a few simple solutions of Laplace's equation. The singularity (or panel) methods presented in the next chapter are based on this idea.

D. THIN SHEAR LAYER EQUATIONS

High Reynolds number flows over airfoils (and other configurations) generate a very thin shear layer (boundary layer) close to the airfoil surface. If δ denotes the boundary layer thickness and x the distance from the leading edge of a flat plate, then it is well-known that

$$\delta(x) \sim \sqrt{\nu x / U} \quad \text{or} \quad \frac{\delta(x)}{x} \sim \sqrt{1 / \text{Re}_x}$$

where ν is the kinematic viscosity and $\text{Re}_x = Ux/\nu$. This formula shows that

$$\frac{\delta(x)}{x} \ll 1 \quad \text{if} \quad \text{Re}_x \gg 1$$

Hence the flow outside of the boundary layer can be considered to be inviscid, but the effect of viscosity cannot be neglected within this layer. Nevertheless, the Navier-Stokes equations

for steady incompressible flow can be simplified because of the fact that δ is much smaller than the representative length of the airfoil (the chord length). This can be deduced from the Navier-Stokes equations as follows:

$$-\frac{1}{\rho} \frac{\partial P}{\partial x} + \nu \left(\frac{\partial^2 u}{\partial x^2} + \frac{\partial^2 u}{\partial y^2} \right) = u \frac{\partial u}{\partial x} + v \frac{\partial u}{\partial y} \quad (2.25)$$

$$-\frac{1}{\rho} \frac{\partial P}{\partial y} + \nu \left(\frac{\partial^2 v}{\partial x^2} + \frac{\partial^2 v}{\partial y^2} \right) = u \frac{\partial v}{\partial x} + v \frac{\partial v}{\partial y} \quad (2.26)$$

u is now replaced by a typical value, say U_e ;

x is now replaced by a typical value, say ℓ ;

y is now replaced by a typical value, say δ .

Then $\frac{\partial u}{\partial y}$ can be expressed by U_e/δ ;

$\frac{\partial u}{\partial x}$ can be expressed by U_e/ℓ ;

$\frac{\partial P}{\partial x}$ can be expressed by $\rho U_e^2/\ell$

(because P and U_e are related by the Bernoulli equations).

Therefore the x-component terms of the Navier-Stokes equation can be estimated to have the following magnitudes:

$$-\frac{1}{\rho} \frac{\partial P}{\partial x} + \nu \left(\frac{\partial^2 u}{\partial x^2} + \frac{\partial^2 u}{\partial y^2} \right) = u \frac{\partial u}{\partial x} + v \frac{\partial u}{\partial y}$$

$$\frac{U_e^2}{\ell}$$

$$\frac{U_e^2}{\ell}$$

$$\frac{U_e^2}{\ell}$$

The magnitude of the term $v \frac{\partial u}{\partial y}$ follows from the application of the continuity equation $\frac{\partial u}{\partial x} + \frac{\partial v}{\partial y} = 0$, i.e., $\frac{U_e}{\ell} + \frac{v}{\delta} = 0$ or $v \sim \frac{\delta U_e}{\ell}$ and therefore

$$v \frac{\partial u}{\partial y} \sim \delta \frac{U_e}{\ell} \frac{U_e}{\delta} \sim \frac{U_e^2}{\ell}$$

The two viscous terms are of vastly different magnitude because $\partial^2 u / \partial x^2 \sim U_e / \ell^2$ and $\partial^2 u / \partial y^2 \sim U_e / \delta^2$ hence $\partial^2 u / \partial y^2 \gg \partial^2 u / \partial x^2$ and $\partial^2 u / \partial x^2$ can therefore be neglected compared to $\partial^2 u / \partial y^2$. Finally, the term $v \partial^2 u / \partial y^2$ must be of the same magnitude as the other terms if the influence of viscosity is to be retained. The y-component terms of the Navier-Stokes equations are easily estimated to be smaller than the x-component terms because

$$u \frac{\partial v}{\partial x} \sim U_e^2 \frac{\delta}{\ell^2} \quad v \frac{\partial v}{\partial y} \sim \frac{U_e^2}{\ell^2} \delta$$

and hence are smaller by a factor $\frac{\delta}{\ell}$. Therefore the two equations reduce to

$$u \frac{\partial u}{\partial x} + v \frac{\partial u}{\partial y} = - \frac{1}{\rho} \frac{\partial P}{\partial x} + \nu \frac{\partial^2 u}{\partial y^2} \quad (2.27)$$

$$\frac{\partial P}{\partial y} = 0 \quad (2.28)$$

By adding the continuity equation (Eq. (2.23)) to these relations, we get the basic equations to describe laminar flow thin shear layers.

E. TURBULENT FLOW

We must deal with the instantaneous properties in the turbulent flow. Thus the time-mean value concept is applied:

$$u = \bar{u} + u'$$

where \bar{u} is the time-mean value, and u' is the fluctuating portion. Similarly,

$$v = \bar{v} + v'$$

$$p = \bar{p} + p'$$

Introducing these relations into Eq. (2.20)

$$\begin{aligned} \bar{u} \frac{\partial \bar{u}}{\partial x} + \bar{v} \frac{\partial \bar{u}}{\partial y} = & - \frac{1}{\rho} \frac{\partial \bar{p}}{\partial x} + \nu \left(\frac{\partial^2}{\partial x^2} + \frac{\partial^2}{\partial y^2} \right) \bar{u} \\ & - \frac{\partial \overline{u'u'}}{\partial x} - \frac{\partial \overline{u'v'}}{\partial y} \end{aligned} \quad (2.29)$$

We can see that $\rho \overline{u'u'}$ and $\rho \overline{u'v'}$ correspond to a normal stress and a shear stress. We call these terms turbulent stresses or Reynolds stresses.

Similar analyses can be done for the y-component equations and z-component equations in the three-dimensional case. The extra Reynolds stresses can be summarized by the following array,

$$\begin{vmatrix} \sigma_{xx} & \sigma_{xy} & \sigma_{xz} \\ \sigma_{yx} & \sigma_{yy} & \sigma_{yz} \\ \sigma_{zx} & \sigma_{zy} & \sigma_{zz} \end{vmatrix} \equiv -\rho \begin{vmatrix} \overline{u'^2} & \overline{u'v'} & \overline{u'w'} \\ \overline{u'v'} & \overline{v'^2} & \overline{v'w'} \\ \overline{u'w'} & \overline{v'w'} & \overline{w'^2} \end{vmatrix}$$

Much of the effort in turbulent flow studies centers on the proper modelling of these turbulent terms.

III. PANEL METHOD

A. INTRODUCTION

The panel method was developed in the 1960's at McDonnell Douglas by Smith and Hess as a numerical approach for 2-D and 3-D potential flow problems. This chapter presents the application of the panel method to 2-D problems about one or two bodies. The basic idea consists in representing the flow past a body by a distribution of singularities (sources, sinks, vortices) on the surface such that the body surface becomes a streamline.

The numerical approach requires some approximations (the assumption given in parentheses refers to our approach).

- A. The surface of the body is replaced by a finite number of elements (straight-line-elements).
- B. The condition of tangential flow is satisfied at a finite number of points, the so-called control-points (midpoints of elements).
- C. The singularity distribution of each element is approximated by some kind of analytical functions (singularity strengths are assumed to be constant along any one element, but vary from element to element).

The advantages of the panel method in comparison with other procedures are:

- A. The panel method does not include an approximation in the physics--thin airfoil theory does.
- B. The panel method can be easily applied to both 2-D and 3-D problems--a virtually unsolvable task for conformal mapping procedures, which are confined to 2-D configurations only.

- C. The panel technique can be readily extended to flow fields past several bodies--a task which causes at least some troubles in "classical" mapping techniques.

The method's versatility has been proven in various extensions, e.g., hydrofoils, cascades, nozzles, and even complete aircraft. Since its origin the method has been improved by features like higher order approximations to both body surface and singularity distribution, taking account for compressibility effects, and inclusion of wake models. Today the panel method is probably our most powerful tool in analyzing potential flows.

B. NONLIFTING FLOW PAST A BODY

The effects of lift (respectively, camber and angle of attack) and displacement (resp. thickness) can be studied separately because of the linearity of Laplace's equation. This section is concerned about displacement flows due to the thickness of bodies, a flow which is usually represented by sources and sinks.

We will first draw the reader's attention to a single straight-line-element, along which sources of constant strength are distributed. This simple case allows us to explain the basics of the panel technique. The source strength λ is defined as the volume of fluid discharged per unit area. Since fluid is ejected perpendicular to the panel's surface in both directions, discharge velocities are half of the source strength. The boundary condition for an inclined panel requires

that the normal component of the free stream velocity is balanced by this discharge velocity (see Figure 3.1).

$$\frac{\lambda}{2} = -V_{\infty} \cos \beta \quad (3.1)$$

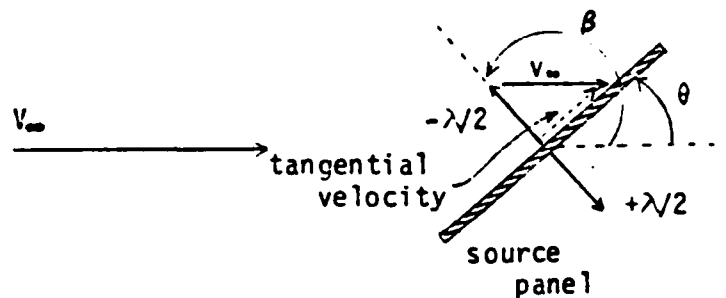


Figure 3.1. Boundary Condition at One Inclined Panel

This relation between a geometric quantity (β) and the unknown source strength establishes tangential flow on the panel surface.

Things, which are obvious for a single panel, become slightly more complicated for a structure of panels. Mutual interference of source panels, i.e., each panel induces a velocity at other panels, causes the complication. While the boundary condition of a single panel had been set up by glancing at a simple geometry sketch, we now better switch to a systematic procedure, emphasizing the concepts of velocity potential and superposition. We consider a 2-D closed body,

approximated by several panels and inclined at an angle to the oncoming flow. Our goal is to derive a relation for the unknown source strengths from the condition of tangential flow at the control points. To this end we will give the velocity potentials of a single source, a source panel, and a closed body built up by a source panel, in that order.

Radial streamlines and concentric circular equipotentials characterize one of the very basic potential flows, the single source flow. Its velocity potential is defined by

$$\text{single source} \quad \phi(x,y) = \frac{\lambda}{2\pi} \ln r \quad (3.2)$$

where r is the distance from (x,y) to the source. Arranging single sources on a straight line element corresponds in terms of the velocity potential to a summation of single potentials, in the limit of an infinite number of sources to an integration over the panel length. Thus the velocity potential of a source panel can be written as

$$\text{source panel} \quad \phi(x,y) = \frac{\lambda}{2\pi} \int_0^{\ell} \ln r \, dS \quad (3.3)$$

m source panels, representing a body, induce a flow field, whose velocity potential at any point (x,y) is given by

$$\phi(x,y) = \sum_{j=1}^m \phi_j(x,y) = \sum_{j=1}^m \frac{\lambda_j}{2\pi} \int_0^{\ell_j} \ln r_j \, dS_j \quad (3.4)$$

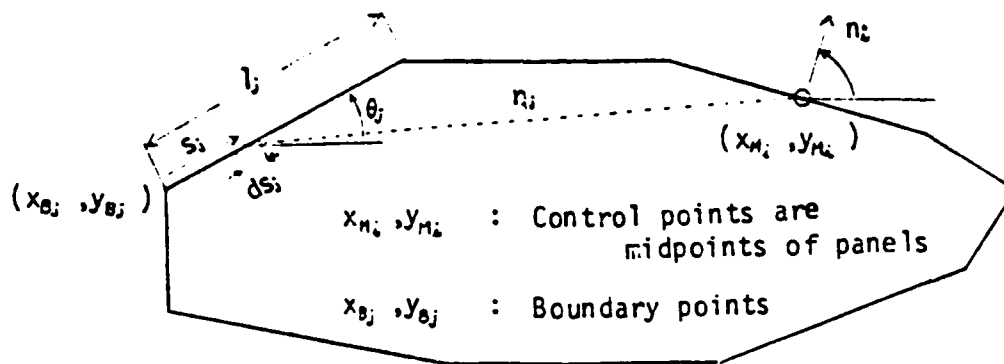


Figure 3.2. Designations for Calculation

We call ϕ the potential of the flow disturbances due to the displacement flow. The total velocity potential of a nonlifting flow results from a superposition of this displacement flow and a uniform flow, which is inclined at an angle α to the x-axis.

$$\phi(x,y) = V_{\infty} \cos \alpha x + V_{\infty} \sin \alpha y + \sum_{j=1}^m \frac{\lambda_j}{2\pi} \int_0^{l_j} \ln r_j \, dS_j$$

Recalling the definition of the velocity potential (velocity equals gradient of potential), the boundary condition of tangential flow takes the form

$$\frac{\partial \phi}{\partial n} = 0 \quad \text{on the surface}$$

Applying this condition within the framework of the panel method provides a system of equations,

$$V_{\infty} \cos \alpha \cos \beta_i + V_{\infty} \sin \alpha \sin \beta_i + \sum_{j=1}^m \frac{\lambda_j}{2\pi} \int_0^{\ell_j} \frac{\partial}{\partial n_i} (\ln r_{ij}) dS_j = 0$$

$$\text{for } i = 1, \dots, m \quad (3.5)$$

which establishes zero normal velocity at all control points. This linear system can be solved for the unknown source strengths after the integrals have been evaluated.

Concept of influence coefficients

The influence coefficient, I_{ij} , is defined as the normal velocity at the i^{th} panel due to a source distribution of 2π -strength at the j^{th} panel.

$$I_{ij} = \int_j \frac{\partial}{\partial n_i} (\ln r_{ij}) dS_j \quad (3.6)$$

The contribution to the normal velocity at the i^{th} panel by the actual source distribution of the j^{th} panel is the product of $\lambda_j/2\pi$ and the influence coefficient I_{ij} . To compute the influence coefficient we must substitute

$$r_{ij} = \sqrt{(x_{M_i} - x_j)^2 + (y_{M_i} - y_j)^2}$$

in Eq. (3.6) and carry out the differentiation.

$$I_{ij} = \int_0^{\ell_j} \frac{(x_{M_i} - x_j)(\partial x_i / \partial n_i) + (y_{M_i} - y_j)(\partial y_i / \partial n_i)}{(x_{M_i} - x_j)^2 + (y_{M_i} - y_j)^2} dS_j \quad (3.7)$$

where

$$\frac{\partial x_i}{\partial n_i} = \cos \beta_i$$

$$\frac{\partial y_i}{\partial n_i} = \sin \beta_i$$

$$x_j = x_{B_j} + S_j \cos \theta_j$$

$$y_j = y_{B_j} + S_j \sin \theta_j$$

The integration covers the length of the j^{th} panel. Finally we obtain

$$I_{ij} = \int_0^{l_j} \frac{[x_{M_i} - (x_{B_j} + S_j \cos \theta_j)] \cos \beta_i + [y_{M_i} - (y_{B_j} + S_j \sin \theta_j)] \sin \beta_i}{[x_{M_i} - (x_{B_j} + S_j \cos \theta_j)]^2 + [y_{M_i} - (y_{B_j} + S_j \sin \theta_j)]^2} dS_j \quad (3.8)$$

Equation (3.8) is expressed in terms of S_j only and, after some manipulations, the integral may be written in the form

$$I_{ij} = \int_0^{l_j} \frac{b - cS_j}{S_j^2 - eS_j + f} dS_j \quad (3.9)$$

where

$$b = (x_{M_i} - x_{B_j}) \cos \beta_i + (y_{M_i} - y_{B_j}) \sin \beta_i$$

$$c = \cos \theta_j \cos \beta_i + \sin \theta_j \sin \beta_i$$

$$e = 2 \cos \theta_j (x_{M_i} - x_{B_j}) + 2 \sin \theta_j (y_{M_i} - y_{B_j})$$

$$f = (x_{M_i} - x_{B_j})^2 + (y_{M_i} - y_{B_j})^2$$

The integration can now be performed analytically,

$$I_{ij} = -\frac{c}{2} [\ln |s_j^2 - e s_j + f|]_0^{\ell_j} + \frac{2b - ce}{\sqrt{4f - e^2}} \left[\arctan \frac{2s_j - e}{\sqrt{4f - e^2}} \right]_0^{\ell_j} \quad (3.10)$$

Determination of unknown source strengths λ

Equation (3.5), expressed in terms of Eq. (3.9) and divided by V_∞ , takes the form

$$\pi \lambda'_i + \sum_{\substack{j=1 \\ j \neq i}}^m \lambda'_j I_{ij} = -\cos \alpha \cos \beta_i - \sin \alpha \sin \beta_i \quad (3.11)$$

where

$$\lambda'_j = \frac{\lambda_j}{2\pi V_\infty}$$

or in the more convenient matrix form

$$\begin{bmatrix} I_{11} & I_{12} & \dots & I_{1m} \\ I_{21} & & & \\ \vdots & & & \\ I_{m1} & & & I_{mm} \end{bmatrix} \begin{bmatrix} \lambda'_1 \\ \lambda'_2 \\ \vdots \\ \lambda'_m \end{bmatrix} = \begin{bmatrix} -\cos \alpha \cos \beta_1 - \sin \alpha \sin \beta_1 \\ -\cos \alpha \cos \beta_2 - \sin \alpha \sin \beta_2 \\ \vdots \\ -\cos \alpha \cos \beta_m - \sin \alpha \sin \beta_m \end{bmatrix} \quad (3.12)$$

The above set of linear equations can be solved for λ_j' by Gauss' elimination method or any other linear equation algorithm.

On-body velocities

The velocity at the midpoint of the i^{th} panel, V_{S_i} can be obtained by a spatial derivative of the velocity potential in tangential direction.

$$\begin{aligned} V_{S_i} &= \frac{\partial \phi(x_i, y_i)}{\partial S_i} \\ &= V_\infty \left(\cos \alpha \frac{\partial x_i}{\partial S_i} + \sin \alpha \frac{\partial y_i}{\partial S_i} + \sum_{j=1}^m \lambda_j' \int_j \frac{\partial (\ln r_{ij})}{\partial S_i} dS_j \right) \end{aligned} \quad (3.13)$$

where

$$\frac{\partial x_i}{\partial S_i} = \cos \theta_i$$

$$\frac{\partial y_i}{\partial S_i} = \sin \theta_i$$

Therefore

$$\left(\frac{V_S}{V_\infty} \right)_i = \cos \alpha \cos \theta_i + \sin \alpha \sin \theta_i + \sum_{j=1}^m \lambda_j' J_{ij} \quad (3.14)$$

where $J_{ij} \equiv \int_j \frac{\partial}{\partial S_i} (\ln r_{ij}) dS_j$ denotes the tangential velocity at the i^{th} panel due to a source distribution of 2π -strength at the j^{th} panel.

The calculation of J_{ij} follows the same procedure as that of I_{ij} , so

$$J_{ij} = \int_0^{\ell_j} \frac{b - c s_j}{s_j^2 - e s_j + f} ds_j \quad (3.15)$$

where

$$b = (x_{M_i} - x_{B_j}) \cos \theta_i + (y_{M_i} - y_{B_j}) \sin \theta_i$$

$$c = \cos \theta_j \cos \theta_i + \sin \theta_j \sin \theta_i$$

$$e = 2 \cos \theta_j (x_{M_i} - x_{B_j}) + 2 \sin \theta_j (y_{M_i} - y_{B_j})$$

$$f = (x_{M_i} - x_{B_j})^2 + (y_{M_i} - y_{B_j})^2$$

Positive signs of on-body velocities indicate that velocities are oriented in the direction of the surface coordinates, while negative signs indicate opposite directions of velocities and surface coordinates. The positive direction of surface coordinates is defined clockwise. Therefore positive values of on-body velocities are to be expected on the upper surface, negative values on the lower surface.

Off-body velocities

Streamlines can be determined by computing velocities at off-body points and using a numerical quadrature to progress

from one point to another point on a streamline. The velocity components can be expressed according to

$$U(x_i, y_i) = \frac{\partial \phi(x_i, y_i)}{\partial x_i} = V_\infty \cos \alpha + \sum_{j=1}^m \frac{\lambda_j}{2\pi} \int_j \frac{\partial}{\partial x_i} \ln r_{ij} dS_j$$

$$V(x_i, y_i) = \frac{\partial \phi(x_i, y_i)}{\partial y_i} = V_\infty \sin \alpha + \sum_{j=1}^m \frac{\lambda_j}{2\pi} \int_j \frac{\partial}{\partial y_i} \ln r_{ij} dS_j$$

Normalizing the above equations by the free stream velocity and abbreviating the integrals simplify the relations to

$$\frac{U(x_i, y_i)}{V_\infty} = \cos \alpha + \sum_{j=1}^m \lambda_j^* I_{ij}^x \quad (3.16)$$

$$\frac{V(x_i, y_i)}{V_\infty} = \sin \alpha + \sum_{j=1}^m \lambda_j^* I_{ij}^y \quad (3.17)$$

I_{ij}^x and I_{ij}^y are again influence coefficients, whose evaluation can be adopted from the already introduced procedure.

$$I_{ij}^x = \int_0^{\ell_j} \frac{b_x - C_x S_j}{S_j^2 - e S_j + f} dS_j \quad (3.18)$$

$$I_{ij}^y = \int_0^{\ell_j} \frac{b_y - C_y S_j}{S_j^2 - e S_j + f} dS_j \quad (3.19)$$

where

$$b_x = x_i - x_{B_j} \quad b_y = y_i - y_{B_j}$$

$$C_x = \cos \theta_j \quad C_y = \sin \theta_j$$

$$e = 2[(x_i - x_{B_j}) \cos \theta_j + (y_i - y_{B_j}) \sin \theta_j]$$

$$f = (x_i - x_{B_j})^2 + (y_i - y_{B_j})^2$$

C. CIRCULATORY FLOW

While inviscid 2-D flow theories are not capable of predicting drag characteristics, information about lift can be provided by them. Creation of lift is closely related to a type of flow called circulatory flow. We mentioned already that the flow around a lifting airfoil can be decomposed into two elementary flows, i.e., displacement flow and circulatory flow. Circulation and circulatory flows are the subjects of this section.

The early approaches of airfoil theory emphasized a flow model in which the airfoil was represented by an infinitely thin vortex sheet only. This so-called thin airfoil theory predicts lift quite well, because lift depends primarily on circulatory flow. Unfortunately a straightforward extension of vortex sheets to "surface singularity" method is impossible. Therefore aerodynamicists have proposed a couple of flow models,

which allow the implementation of circulatory flows in "surface-singularity" methods. Examples are:

- (1) Smith and Hess represent circulatory flows by a combination of source and vortex distributions. [Ref. 1]
- (2) Martensen prefers vortex distributions only, but states the problems in terms of the stream function. [Ref. 2]
- (3) Davenport makes use of linearly varying vortex distributions. [Ref. 3]

Our approach follows the ideas of Smith and Hess. These circulatory flows are composed of a vortex distribution, which is constant along all and for all panels, and a source distribution of conventional shape.

We start at the very beginnings of vortex flows. Concentric circular streamlines and radial equipotentials characterize the flow field of a single vortex. Its velocity potential can be written as

$$\text{single vortex } \phi(x,y) = - \frac{\Gamma}{2\pi} \arctan \frac{y-y_v}{x-x_v} \quad (3.20)$$

with (x_v, y_v) as the center of the vortex. A structure of m vortex panels induces a flow field, whose velocity potential at any point (x,y) is given by

$$\phi(x,y) = \Gamma \sum_{j=1}^m \left(- \frac{1}{2\pi} \right) \int_0^{\ell_j} \arctan \frac{y-y_j}{x-x_j} dS_j \quad (3.21)$$

This flow field differs in two important points from the non-lifting flow field:

- (1) It violates the condition of tangential flow.
- (2) The unknown singularity strength Γ cannot be determined immediately.

The task of determining circulation must be postponed to the implementation of the Kutta condition. Temporarily we set the vortex strength equal to one. Tangential flow must be established by the aid of an additional source distribution. Strengths of this additional source distribution must be computed according to the condition that the normal velocities due to the vortex distributions at the control points are balanced by the normal velocities due to the additional source distribution.

$$\sum_{j=1}^m \frac{\lambda_j}{2\pi} \int_j \frac{\partial}{\partial n_i} \ln(r_{ij}) dS_j = \sum_{j=1}^m \int_j \frac{\partial}{\partial n_i} \left(\tan^{-1} \frac{y_i - y_j}{x_i - x_j} \right) dS_j$$

Abbreviating the integrals by the above defined influence coefficients, we get

$$\sum_{j=1}^m \lambda_j^{(1)} I_{ij}^{(s)} = - \sum_{j=1}^m I_{ij}^{(v)} \quad \text{for } i = 1, \dots, m \quad (3.22)$$

where

$\lambda_j^{(1)}$ are the unknown strengths whose effect is intended to balance the normal velocities induced by a unit vortex distribution.

$I_{ij}^{(s)}$ is the normal influence coefficient due to a source distribution.

$I_{ij}^{(v)}$ is the normal influence coefficient due to a vortex distribution.

$J_{ij}^{(s)}$ is the tangential influence coefficient due to a source distribution.

$J_{ij}^{(v)}$ is the tangential influence coefficient due to a vortex distribution.

Since influence coefficients of source and vortex distributions are related by $I_{ij}^{(v)} = -J_{ij}^{(s)}$, the above equation can be expressed according to

$$\sum_{j=1}^m \lambda_j^{(1)} I_{ij}^{(s)} = \sum_{j=1}^m J_{ij}^{(s)} \quad \text{for } i = 1, \dots, m \quad (3.23)$$

By solving this system for $\lambda_j^{(1)}$, we determine the properties of circulatory flow of unit strength.

Calculation of disturbance velocity due to unit circulatory flow

The disturbance velocity, $V_i^{(v)}$, is composed of two parts, one due to the constant vortex distribution, the other due to the additional source distribution

$$V_i^{(v)} = 1 \sum_{j=1}^m J_{ij}^{(v)} + \sum_{j=1}^m \lambda_j^{(1)} J_{ij}^{(s)} \quad (3.24)$$

Making use again of the relation between influence coefficients ($J_{ij}^{(v)} = I_{ij}^{(s)}$), we have

$$V_i^{(v)} = \sum_{j=1}^m I_{ij}^{(s)} + \sum_{j=1}^m \lambda_j^{(1)} J_{ij}^{(s)} \quad (3.25)$$

D. SYNTHESIZING A COMBINED FLOW

The Kutta condition serves as matching condition for nonlifting and circulatory flow. These two basic flows must be

superimposed such that flows of upper and lower surface merge smoothly at the trailing edge. This original version of the Kutta condition is usually substituted by the condition of zero load (or equal velocities on both upper and lower surface) at the trailing edge (see Figure 3.3).

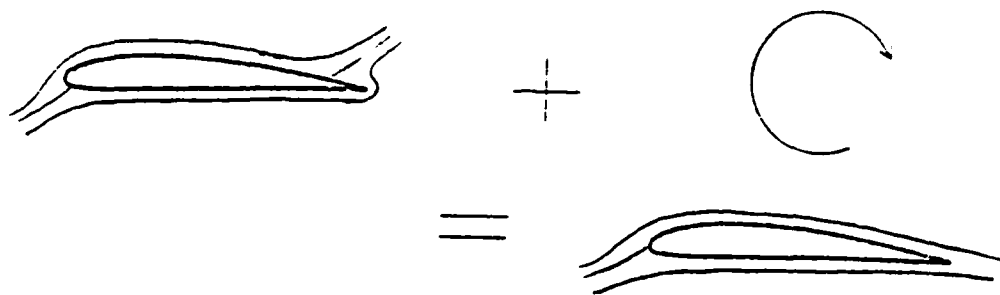


Figure 3.3. Single Airfoil: Superposition of Nonlifting and Circulatory Flow, Controlled by the Kutta Condition

Since the panel method does not permit the evaluation of velocities at the trailing edge, the Kutta condition is satisfied approximately by requiring that velocities at the control points of the rearmost panels have equal magnitude. Therefore the rearmost panels should be chosen short so that flow at their midpoints will effectively represent that at the trailing edge.

Determination of circulation

Suppose 1^{st} and m^{th} panels are the closest panels to the trailing edge on the lower and upper surface, then we can write the

Kutta condition as

$$-V_1^{(N)} - \Gamma V_1^{(v)} = V_m^{(N)} + \Gamma V_m^{(v)} \quad (3.26)$$

where $V_i^{(N)}$ denotes the tangential velocity in nonlifting flow.

Equation (3.26) can be solved for the circulation Γ .

Calculation of on-body velocities and of pressure coefficients

Three parts contribute to the total velocity: free stream, disturbance due to displacement flow and disturbance due to lifting flow. Say $V^{(N)}$ designates the velocity due to the nonlifting flow including the free stream component and $V^{(v)}$ represents the velocity due to a lifting flow of unit circulation. Then the total tangential velocity at the midpoint of the i^{th} panel is given by

$$V_i = V_i^{(N)} + \Gamma V_i^{(v)} \quad (3.27)$$

Once the velocity has been computed, the pressure, customarily expressed by means of a dimensionless coefficient C_p , is determined by Bernoulli's equation:

$$C_{P_i} = \frac{P_i - P_\infty}{\frac{1}{2} \rho V_\infty^2} = 1 - \left(\frac{V_i}{V_\infty}\right)^2 \quad (3.28)$$

Addendum: More than one body configuration.

One of the main advantages of the panel method is its easy extension to multi-element airfoils. As a matter of

fact even flow past an infinite number of bodies can be solved by means of the panel method, if these bodies are arranged in form of cascades. The minor changes, which are necessary to apply the panel method to a finite number of bodies, include:

- (1) The overall scheme must provide a circulatory flow for each lifting body. (The number of nonlifting flows remains one.)
- (2) Flow past each body with lift is subject to a Kutta condition. Accordingly the numbers of equations requiring zero load at the trailing edge equals the number of circulatory flows, which allows the definite determination of each lifting body's circulation.

Figure 3.4 illustrates the superposition of nonlifting and circulatory flows for a two element airfoil.

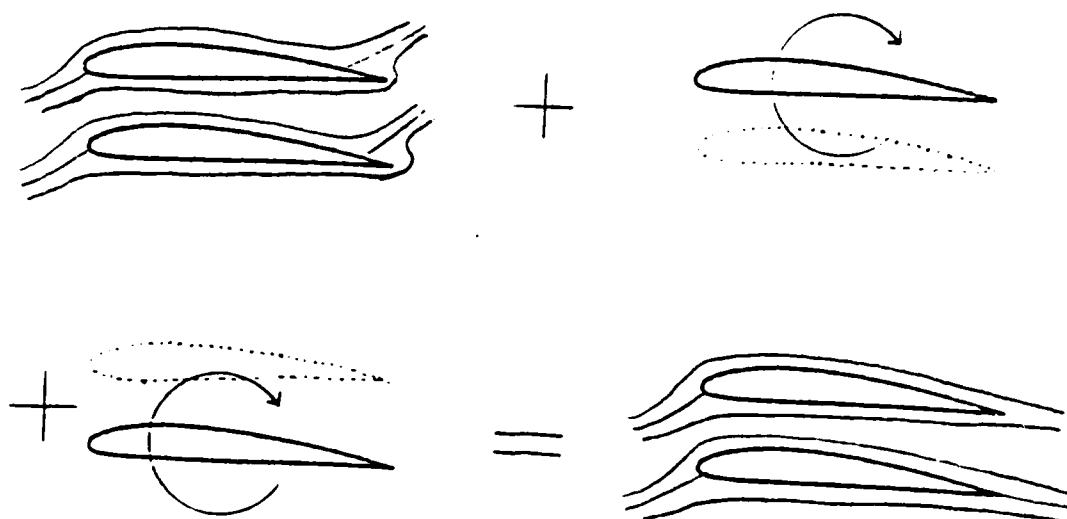


Figure 3.4. Two Element Airfoil: Superposition of Nonlifting and Circulatory Flows

E. EXAMPLES

This section illustrates the capabilities of the program "PANEL" which can be applied to 2-D potential flow problems past one or two bodies.

Flow past one circular cylinder

The source panel technique is applied to the flow past a circular cylinder. This case is regarded as nonlifting, i.e., the cylinder experiences no force perpendicular to the free stream. As sketched in Figure 3.5, the surface of the cylinder is approximated by eight panels of equal width. For zero angle of attack, Eq. (3.5) reduces to

$$V_{\infty} \cos \beta_i + \frac{\lambda_i}{2} + \sum_{\substack{j=1 \\ j \neq i}}^m \frac{\lambda_j}{2\pi} \int_j \frac{\partial (\ln r_{ij})}{\partial n_i} dS_j = 0 \quad (3.29)$$

Solving a set of 8 simultaneous algebraic equations, the source strengths and the pressure coefficients can be determined.

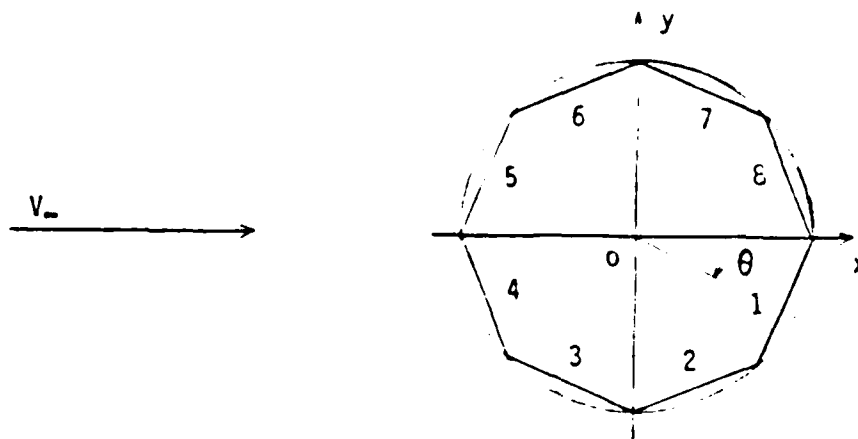


Figure 3.5. Arrangement of Panels on a Circular Cylinder

The results are shown in Figure 3.6 where they are compared with analytical results ($C_p = 1 - 4\sin^2\theta$).

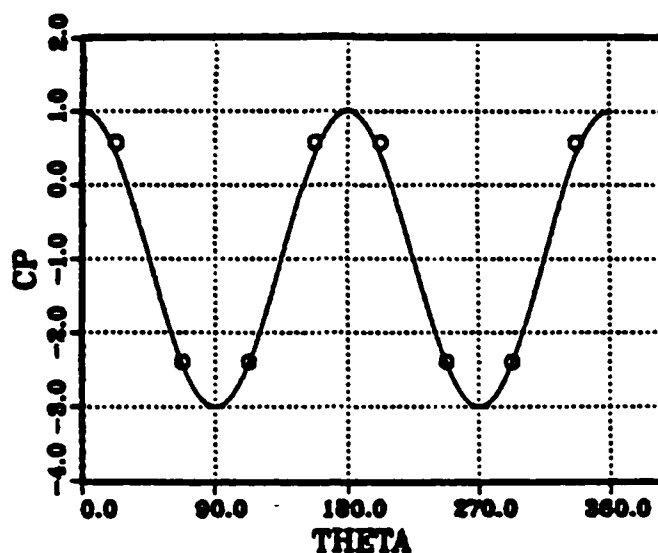


Figure 3.6. Pressure Coefficient on a Circular Cylinder Obtained by Using Eight Source Panels (Marked by 0) in Comparison with the Exact Solution

This example demonstrates the power of the panel method. However the reader should be aware that only 8 panels are not sufficient to describe the geometry in most of the cases. Basically the achieved accuracy depends on both the shape of the body and the panel configuration (number of panels and local widths). A closer spacing is advisable in regions where severe changes of the pressure distribution are expected (e.g., leading edge).

Flow past a pair of circular cylinders

Two circular cylinders are arranged side-by-side in a uniform stream. The surface of each cylinder is replaced by 50 panels of equal width (see Figure 3.7(a)). The computed velocity distribution on one of the cylinders is shown in Figure 3.8(b). The reader shall pay some attention to a comparison between the flow past one and the flow past a pair of cylinders. Obviously the maximum velocity is increased by the existence of a second cylinder. The closer the two cylinders are arranged, the higher the maximum velocity. While the stagnation points in a single cylinder flow are located at the farthest down and upstream points of the cylinder, the disturbance of a second cylinder causes the stagnation points to move towards the other cylinder. The streamline picture, given in Figure 3.8, should provide a deeper understanding of this kind of flow.

Flow past two element airfoil

The main goal of leading and trailing edge devices is to obtain a higher lift coefficient. We will investigate the effect of a single slotted flap on the pressure distribution of the main airfoil.

The pressure distributions of a single airfoil and of an airfoil-flap combination are compared in Figure 3.9. The coordinates of both main airfoil (a NACA 4412) and flap are listed in Section F (sample input data). The results indicate that lift increases more than 50% by using a slotted, 21.5 degree deflected flap.

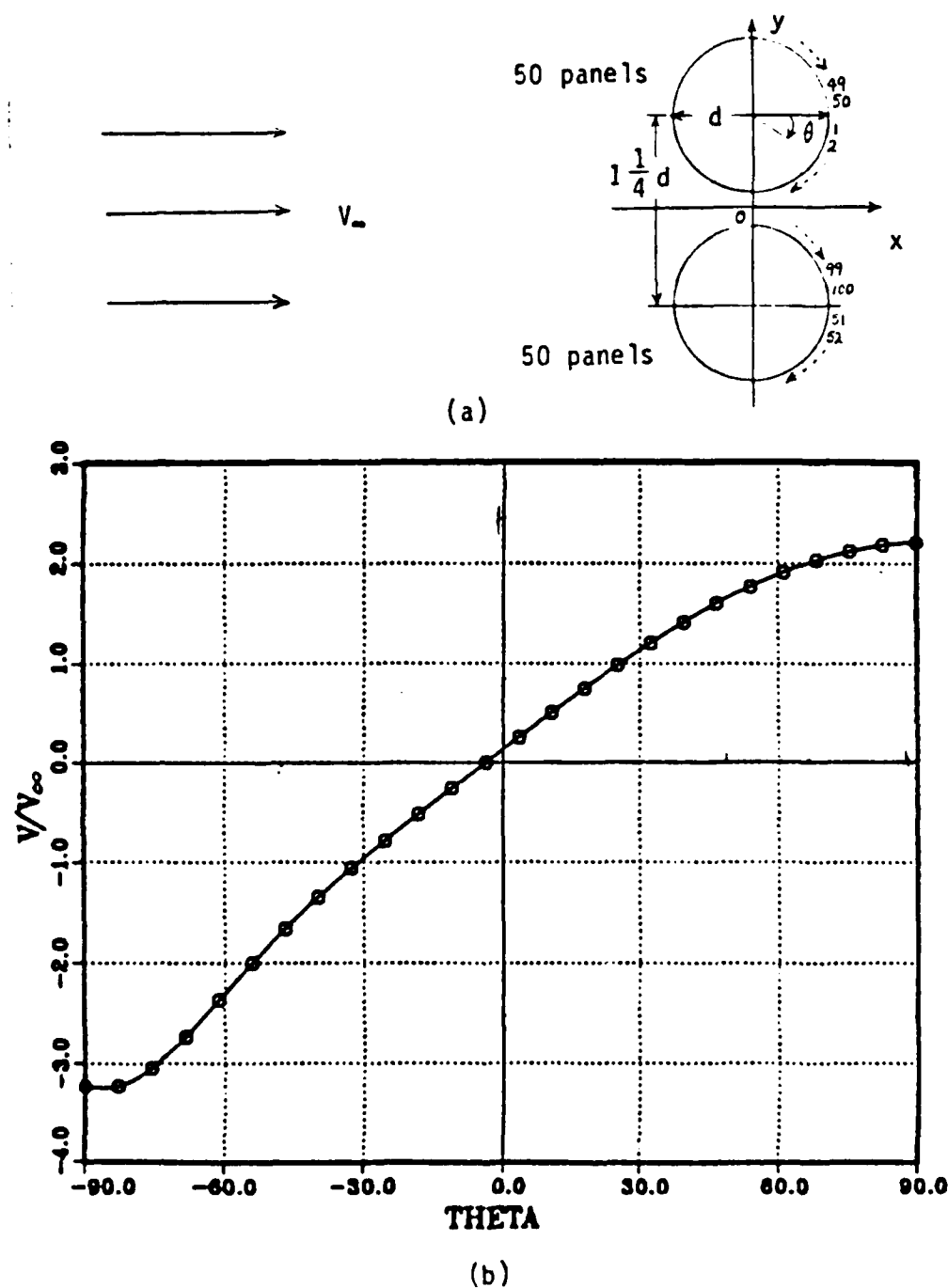


Figure 3.7. (a) Arrangement of Panels on Two Cylinders Side by Side
 (b) Calculated Velocity Distribution on One of Two Identical Circular Cylinders Whose Centers Are One and a Quarter Diameters Apart

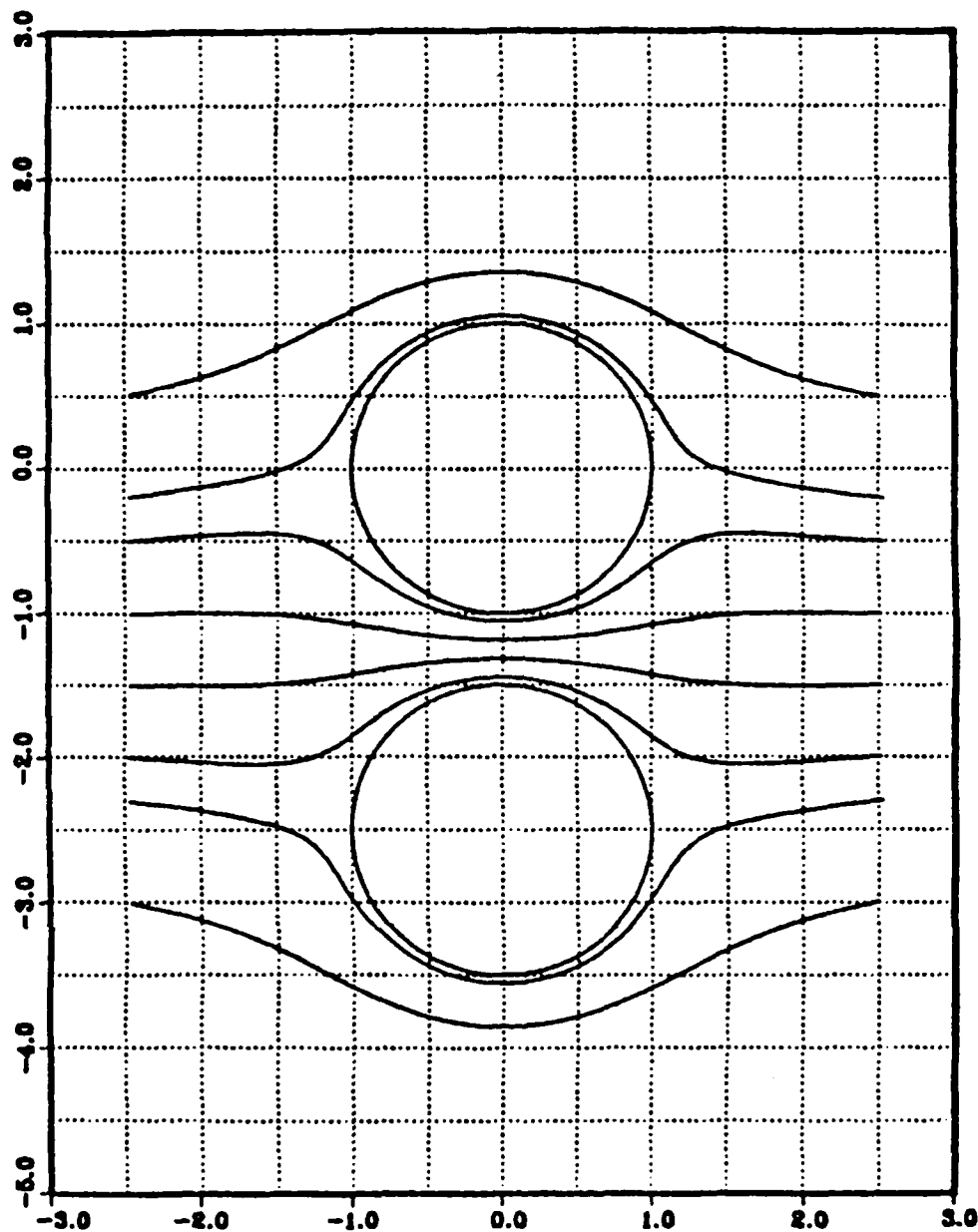


Figure 3.8. Streamlines of Flow Past Two Identical Cylinders Whose Centers Are One and a Quarter Diameters Apart

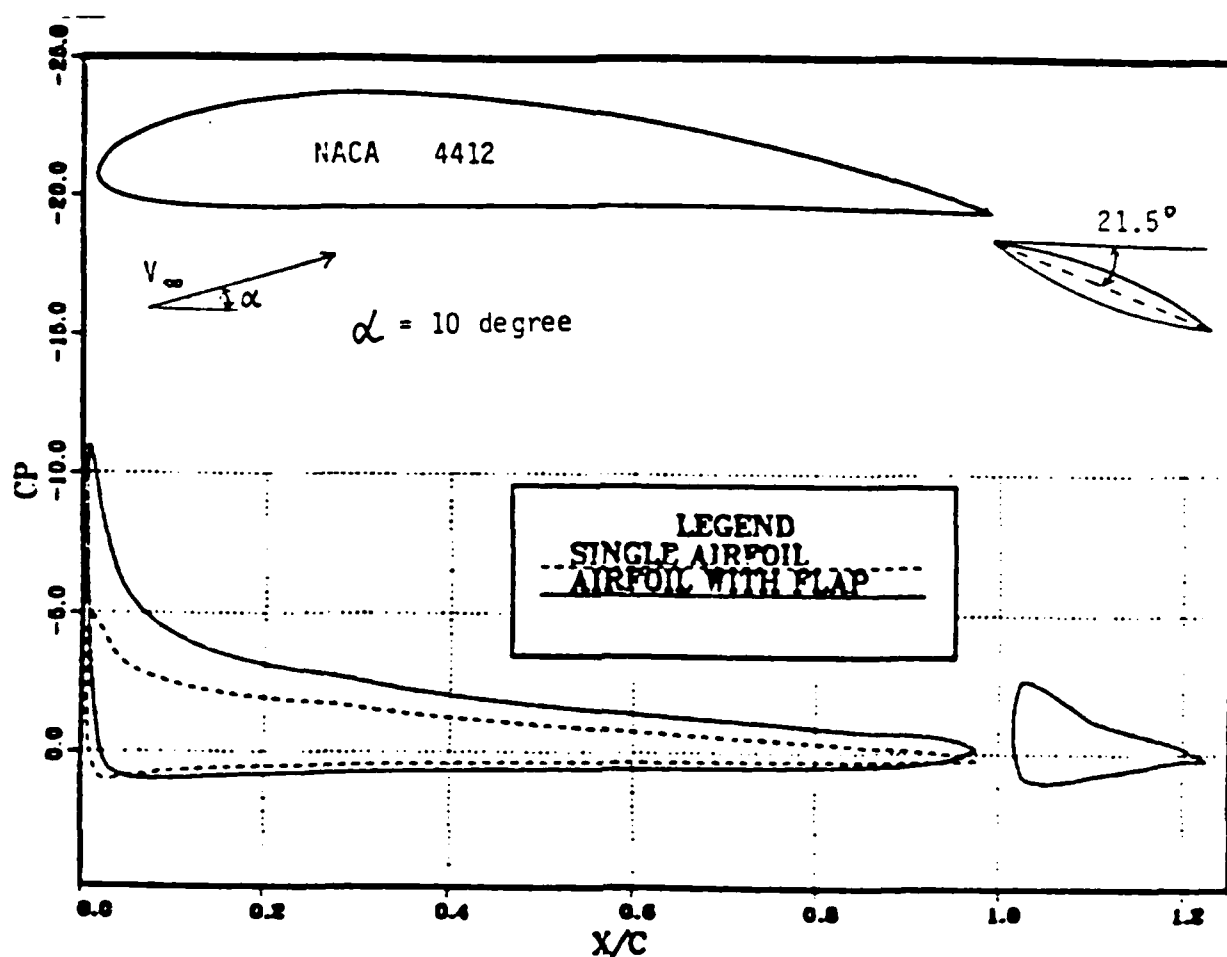


Figure 3.9. Pressure Distributions on a Single and a Flapped Airfoil

Airfoil in ground effect

Flow past an airfoil in ground effect is another application of our program.

The boundary condition at the ground requires vanishing normal velocity there. We meet indirectly this condition by arranging the second, imaginary airfoil such that the ground becomes an axis of symmetry of this "new" flow field (see

Figure 3.10). Since an axis of symmetry must be impermeable to fluid particles, the desired flow is obtained without explicitly satisfying the boundary condition at the ground. This kind of flow is a challenge to aerodynamicists for several reasons. Whenever an airplane takes off and lands, it passes a zone where flow is severely affected by the proximity of the ground. Wind tunnel experiments must be corrected for wall-effects, quite a similar situation with grounds below and above the airfoil. And there was a German experimental seaplane that makes use of flying very close to the sea level. However, our numerical experiments will tell only one part of the story because all these flows are highly 3-dimensional.

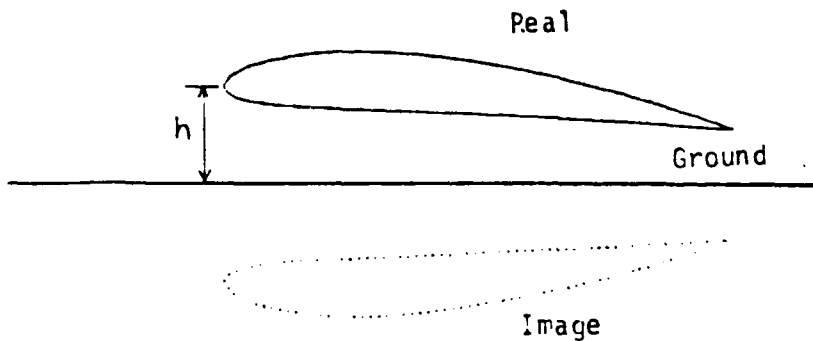


Figure 3.10. Airfoil in Ground Effect

Let's first question how does the pressure distribution change near the ground. Figure 3.11 shows that lift is reduced

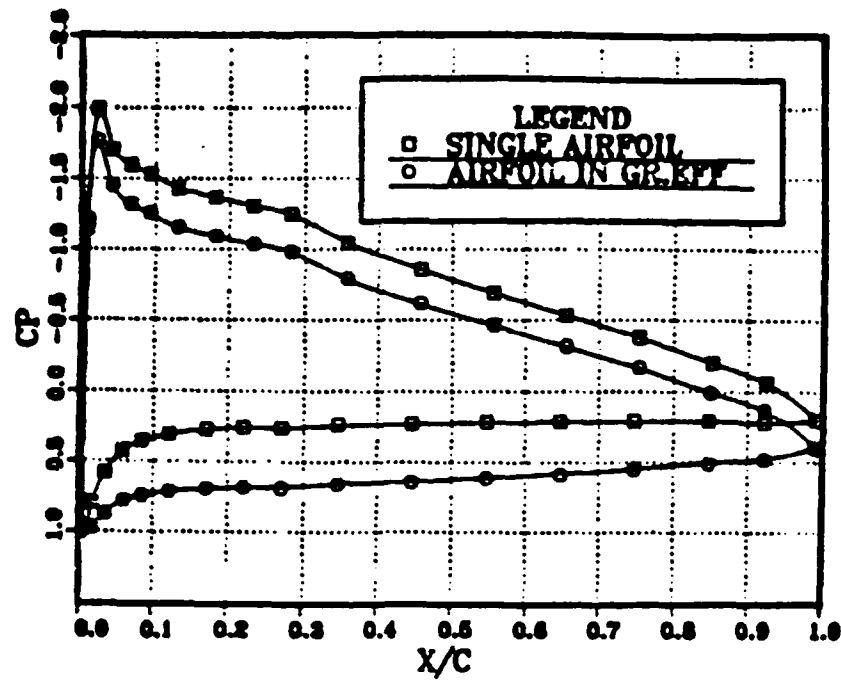


Figure 3.11. Pressure Distributions on a Single NACA 4412 and on a NACA 4412 in Ground Effect ($h/c = 0.2$, $\alpha = 5^\circ$)

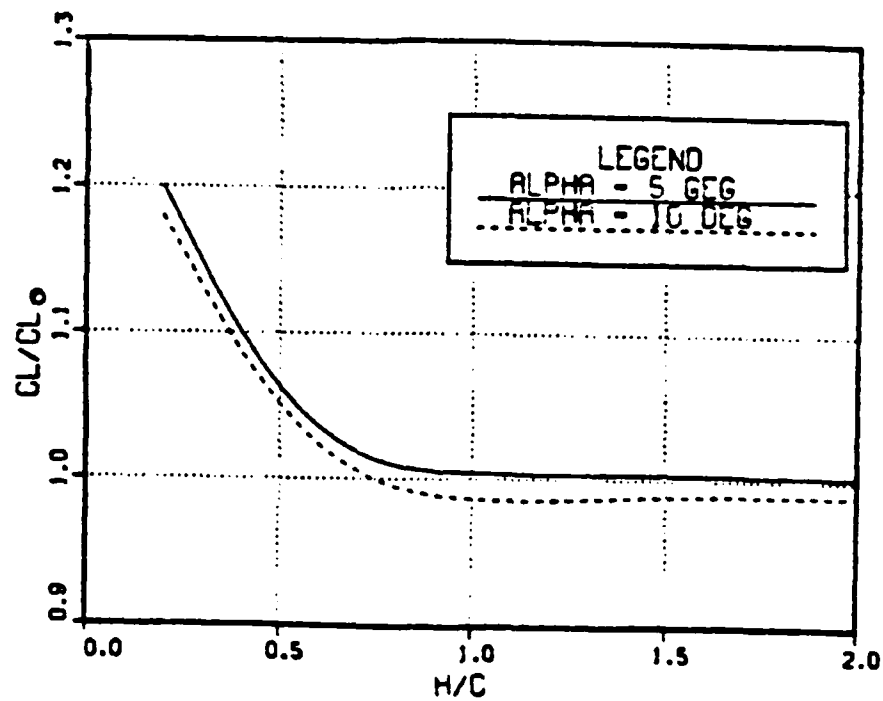


Figure 3.12. The Lift of a NACA 4412 Near the Ground

on the upper surface and increased on the lower surface. In the particular case the overall lift gain is about 15% of the lift in free air, but we might not always expect a lift gain. The actual balance between lift reduction on the upper and lift increase on the lower surface depends on both distance from the ground and angle of incidence. Figure 3.12 confirms that there are cases with less lift than in free air. High angles of attack and moderate distances from ground are susceptible constellations to lift loss.

F. I/O--DESCRIPTION AND LISTING OF THE PROGRAM "PANEL"

This program calculates non-lifting and lifting potential flow past one or two bodies. Any 2-dimensional shape and any angle of attack, which do not cause flow separation, are acceptable.

Input data

The data must be arranged in the following order:

- (1) Header card;
- (2) Coordinates of first body cards (variable number of cards);
- (3) Second body control card;
- (4) Coordinates of second body cards (variable number of cards).

Items 3 and 4 are used only for the 2-body case. The actual instructions are as follows.

Header card

- 1-10: Number of bodies (integer)
11-20: Number of points of the first body (integer)
21-30: Angle of attack in degrees (real)

Coordinates of first body cards

The input procedure of body coordinates requires the following sequence: start at the trailing edge, progress on the lower surface to the leading edge, return on the upper surface to the trailing edge and finish with the trailing edge. The trailing edge of closed bodies is input twice, as first and last point. However airfoils with finite trailing edge thickness should be treated as non-closed bodies, i.e., the last point input is not the first point repeated.

1-10: X coordinates of the points defining the body (real)

11-20: Y coordinates of the points defining the body (real)

Second body control card

1-10: Number of points of the second body

Coordinates of second body card

The X- and Y-coordinates of the 2nd body are input in the same format as the coordinates of the first body.

Output

There are two kinds of solutions, non-lifting and lifting, both of which are preceded by the following column header.

PANEL	X	Y	V	C _p
-------	---	---	---	----------------

where

PANEL is the number of the panel;

X and Y are the coordinates of control points (not boundary points);

V denotes the relative velocity (V/V_∞); and

C_p denotes the pressure coefficient.

Sample problem

This sample illustrates program input and output. The data refer to the airfoil-flap example of Section III.E (see Figure 3.9).

Input

......1.....2.....3.....

2 35 10.

1.	.0
.95	-.0016
.90	-.0022
.80	-.0039
.70	-.0065
.60	-.01
.50	-.014
.40	-.018
.30	-.0226
.25	-.025
.20	-.0274
.15	-.0288
.10	-.0286
.075	-.0274
.05	-.0249
.025	-.0195
.0125	-.0143
.0	.0
.0125	.024
.025	.0339
.05	.0473
.075	.0576
.10	.0659
.15	.0789
.20	.0880
.25	.0941
.30	.0976
.40	.0980
.50	.0919
.60	.0814
.70	.0669
.80	.0489
.90	.0271
.95	.0147
1.0	.0

9	
1.25	-.15
1.20	-.14
1.15	-.125
1.05	-.08
1.0	-.05
1.05	-.06
1.15	-.09
1.20	-.115
1.25	-.15

Output

NONLIFTING SOLUTION

PANEL	XM	YM	V	CP
1	0.97500	-0.00080	-3.05132	-8.31055
2	0.92500	-0.00190	-1.71788	-1.95110
3	0.85000	-0.00305	-1.43382	-1.05583
4	0.75000	-0.00520	-1.20962	-0.46318
5	0.65000	-0.00825	-1.11906	-0.25229
6	0.55000	-0.01200	-1.07063	-0.14625
7	0.45000	-0.01600	-1.03543	-0.07210
8	0.35000	-0.02030	-1.01792	-0.03616
9	0.27500	-0.02380	-0.97360	0.05210
10	0.22500	-0.02620	-0.98044	0.03874
11	0.17500	-0.02810	-0.97498	0.04942
12	0.12500	-0.02870	-0.95981	0.07876
13	0.08750	-0.02800	-0.92944	0.13613
14	0.06250	-0.02615	-0.90437	0.18212
15	0.03750	-0.02220	-0.81613	0.33393
16	0.01875	-0.01690	-0.66716	0.55489
17	0.00625	-0.00715	-0.06604	0.99564
18	0.00625	0.01200	1.20372	-0.44893
19	0.01875	0.02895	1.51674	-1.30050
20	0.03750	0.04060	1.46366	-1.14230
21	0.06250	0.05245	1.45104	-1.10550
22	0.08750	0.06175	1.44313	-1.08263
23	0.12500	0.07240	1.40582	-0.97632
24	0.17500	0.08345	1.38729	-0.92458
25	0.22500	0.09105	1.36530	-0.86405
26	0.27500	0.09585	1.34794	-0.81694
27	0.35000	0.09780	1.24546	-0.55117
28	0.45000	0.09495	1.15851	-0.34214
29	0.55000	0.08665	1.07036	-0.14566
30	0.65000	0.07415	0.96331	0.07203
31	0.75000	0.05790	0.82090	0.32612
32	0.85000	0.03800	0.55160	0.69573
33	0.92500	0.02090	0.37152	0.86197
34	0.97500	0.00735	-0.86208	0.25681
35	1.22500	-0.14500	-2.69341	-6.25447
36	1.17500	-0.13250	-1.67415	-1.80278
37	1.10000	-0.10250	-0.59324	0.64806
38	1.02500	-0.06500	1.34805	-0.81725
39	1.02500	-0.05500	3.04627	-8.27976
40	1.10000	-0.07500	1.49617	-1.23852
41	1.17500	-0.10250	0.51932	0.73031
42	1.22500	-0.13250	-1.15598	-0.33629

LIFTING SOLUTION

PANEL	XM	YM	V	CP
1	0.97500	-0.00080	-1.09525	-0.19958
2	0.92500	-0.00190	-0.80975	0.34430
3	0.85000	-0.00305	-0.71356	0.49083
4	0.75000	-0.00520	-0.65850	0.56638
5	0.65000	-0.00825	-0.63122	0.60157
6	0.55000	-0.01200	-0.60472	0.63432
7	0.45000	-0.01600	-0.56660	0.67897
8	0.35000	-0.02030	-0.52361	0.72583
9	0.27500	-0.02380	-0.47182	0.77738
10	0.22500	-0.02620	-0.43188	0.81348
11	0.17500	-0.02810	-0.35514	0.87387
12	0.12500	-0.02870	-0.22992	0.94714
13	0.08750	-0.02800	-0.07829	0.99387
14	0.06250	-0.02615	0.09794	0.99041
15	0.03750	-0.02220	0.47846	0.77108
16	0.01875	-0.01690	1.09475	-0.19848
17	0.00625	-0.00715	2.42874	-4.89880
18	0.00625	0.01200	3.46087	-10.97764
19	0.01875	0.02895	3.13743	-8.84344
20	0.03750	0.04060	2.71609	-6.37716
21	0.06250	0.05245	2.48044	-5.15257
22	0.08750	0.06175	2.34667	-4.50686
23	0.12500	0.07240	2.20878	-3.87871
24	0.17500	0.08345	2.08988	-3.36759
25	0.22500	0.09105	2.00707	-3.02833
26	0.27500	0.09585	1.94596	-2.78674
27	0.35000	0.09780	1.81808	-2.30540
28	0.45000	0.09495	1.69455	-1.87149
29	0.55000	0.08665	1.60093	-1.56299
30	0.65000	0.07415	1.51477	-1.29451
31	0.75000	0.05790	1.43499	-1.05920
32	0.85000	0.03800	1.33681	-0.78706
33	0.92500	0.02090	1.28943	-0.66263
34	0.97500	0.00735	1.09525	-0.19956
35	1.22500	-0.14500	-0.86324	0.25482
36	1.17500	-0.13250	-0.79007	0.37579
37	1.10000	-0.10250	-0.43515	0.81064
38	1.02500	-0.06500	0.41219	0.83010
39	1.02500	-0.05500	1.91951	-2.68453
40	1.10000	-0.07500	1.49954	-1.24862
41	1.17500	-0.10250	1.23353	-0.52159
42	1.22500	-0.13250	0.86324	0.25482

61


```

C --- CALCULATE INFLUENCE COEFFICIENTS OF NORMAL VELOCITY ---
C
      IF(I.EQ.J) GO TO 15
      B = (XM(I)-XB(J))*COS(BE(I))+(YM(I)-YB(J))*SIN(BE(I))
      C = COS(TH(J))*COS(BE(I))+SIN(TH(J))*SIN(BE(I))
      E = 2.*COS(TH(J))*(XM(I)-XB(J))+2.*SIN(TH(J))*(YM(I)-YB(J))
      F = (XM(I)-XB(J))*2+(YM(I)-YB(J))*2
      H = SQRT(4.*F-E**2)
      Z(I,J) = TEG(B,C,E,F,H,A(J))
15  CONTINUE
      Z(I,I)=3.141592
14  CONTINUE
C --- SOLVE SET OF LINEAR EQUATIONS FOR SOURCE STRENGTHS ---
C
      IDGT = 0
      CALL LEQT2F (Z,1,N,200,V,IDGT,WKAREA,IER)
C --- CALCULATE INFLUENCE COEFFICIENTS OF TANGENTIAL VELOCITY ---
C
      DO 16 I = 1,N
        DO 17 J = 1,N
          IF(I.EQ.J) GO TO 17
          B = (XM(I)-XB(J))*COS(TH(I))+(YM(I)-YB(J))*SIN(TH(I))
          C = COS(TH(J))*COS(TH(I))+SIN(TH(J))*SIN(TH(I))
          E = 2.*COS(TH(J))*(XM(I)-XB(J))+2.*SIN(TH(J))*(YM(I)-YB(J))
          F = (XM(I)-XB(J))*2+(YM(I)-YB(J))*2
          H = SQRT(4.*F-E**2)
          Y(I,J) = TEG(B,C,E,F,H,A(J))
17  CONTINUE
          Y(I,I)=0.0
16  CONTINUE
C --- CALCULATE TOTAL VELOCITY AND CP AT MIDPOINTS OF EACH PANEL ---
C
      WRITE(8,95)
95  FORMAT(///,25X,'NONLIFTING SOLUTION',//
        *10X,'PANEL',5X,'XM',8X,'YM',11X,'V',10X,'CP')
      DO 18 I = 1,N
        S=0.
        DO 19 J = 1,N
          S = S+V(J)*Y(I,J)
19  CONTINUE
          VV(I) = COS(TH(I))*COS(AN)+SIN(TH(I))*SIN(AN)+S
          CP(I) = 1.-VV(I)*2
          WRITE(8,93) I,XM(I),YM(I),VV(I),CP(I)
93  FORMAT(10X,I3,3X,2F10.5,3X,2F10.5)
18  CONTINUE
CCCCCCCCCCCCCCCCCCCCCCCCCCCCCCCCCCCCCCCCCCCCCCCCCCCCCCCCCCCC
C
C          LIFTING PART (1-BODY)
C
CCCCCCCCCCCCCCCCCCCCCCCCCCCCCCCCCCCCCCCCCCCCCCCCCCCCCCCCCCCC
C --- CALCULATE SOURCE STRENGTHS DUE TO CIRCULATORY FLOW OF UNIT
C                                     STRENGTH ---
C
      DO 20 I = 1,N
        S = 0.
        DO 21 J = 1,N
          S = S+Y(I,J)
21  CONTINUE
          V1(I)=S
20  CONTINUE
      IDGT = 0
      CALL LEQT2F (Z,1,N,200,V1,IDGT,WKAREA,IER)

```

```

C
C --- CALCULATE DISTURBANCE VELOCITY DUE TO CIRCULATORY FLOW OF UNIT
C                               STRENGTH ---
C
C      DO 22 I = 1,N
C          S = 0.
C          DO 23 J = 1,N
C              S = S+Y(I,J)*V1(J)+Z(I,J)
C      23 CONTINUE
C          VC(I)=S
C      22 CONTINUE
C
C --- CALCULATE VORTEX STRENGTHS BY KUTTA CONDITION ---
C
C      SI = -(VV(1)+VV(N))/(VC(1)+VC(N))
C
C --- CALCULATE TOTAL VELOCITY AND CP AT MIDPOINTS OF EACH PANEL ---
C
C      WRITE(8,96)
C      96 FORMAT(///,27X,'LIFTING SOLUTION',//
C          *10X,'PANEL',5X,'XM',8X,'YM',11X,'V',10X,'CP')
C      DO 24 I = 1,N
C          VVV(I) = VV(I)+SI*VC(I)
C          CP(I) = 1.-VVV(I)**2
C          WRITE(8,93)I, XM(I),YM(I),VVV(I),CP(I)
C      24 CONTINUE
C      25 FORMAT(3F10.5)
C      GO TO 700
C
C --- READ INPUT DATA (FOR SECOND BODY) ---
C
C      600 READ(4,31) MM
C      31 FORMAT(I10)
C      DO 32 I = NN+1,NN+MM
C          READ(4,11)XB(I),YB(I)
C      32 CONTINUE
C      M = NN+MM-2
C
C --- CALCULATE MID-POINTS OF PANELS AND ANGLES THETA ---
C
C      DO 33 I=N+1,M
C          K = I+1
C          XM(I) = (XB(K)+XB(K+1))/2.
C          YM(I) = (YB(K)+YB(K+1))/2.
C          THH = (YB(K+1)-YB(K))/(XB(K+1)-XB(K))
C          TH(I)= ATAN(THH)
C          IF(XB(K+1).LT.XB(K)) TH(I)=TH(I)+3.141592
C      33 CONTINUE
C
C --- CALCULATE PANEL LENGTHS ---
C
C      DO 34 I = N+1,M
C          K = I+1
C          A(I) = SQRT((XB(K+1)-XB(K))**2+(YB(K+1)-YB(K))**2)
C      34 CONTINUE
C      DO 35 I = N+1,M+1
C          XB(I) = XB(I+1)
C          YB(I) = YB(I+1)
C      35 CONTINUE

```

REPRODUCED AT GOVERNMENT EXPENSES


```

C
C --- CALCULATE VORTEX STRENGTHS BY KUTTA CONDITION ---
C
X1 = VC1(1)+VC1(N)
X2 = VC2(1)+VC2(N)
X3 = -VV(1)-VV(N)
X4 = VC1(N+1)+VC1(M)
X5 = VC2(N+1)+VC2(M)
X6 = -VV(N+1)-VV(M)
SI2 = (X3*X4-X1*X6)/(X4*X2-X1*X5)
SI1 = (X3-X2*SI2)/X1

C
C --- CALCULATE TOTAL VELOCITY AND CP AT MIDPOINTS OF EACH PANEL ---
C
WRITE(8,96)
DO 50 I =1,M
  VT(I) = VC1(I)*SI1+VC2(I)*SI2
  VVV(I) = VV(I)+VT(I)
  CP(I) = 1.-VVV(I)**2
  WRITE(8,93)I,XM(I),YM(I),VVV(I),CP(I)
50 CONTINUE
700 WRITE(6,97)
97 FORMAT(1X,'COMPUTATION COMPLETED')
  STOP
  END

C
C --- THIS FUNTION EVALUATES THE INTEGRALS (INFLUENCE COEFFICIENTS) ---
C
FUNCTION TEG(B,C,P,Q,R,S)
  TERM1 = ALOG((S**2-P*S+Q)/Q)
  TERM2 = ATAN((2.*S-P)/R)-ATAN(-P/R)
  TEG = -C*TERM1/2.+(2.*B-C*P)*TERM2/R
  RETURN
  END

```

IV. BOX METHOD

A. INTRODUCTION

The thin shear layer equations are more complicated than Laplace's equation because they are nonlinear. This chapter presents the box-method, which can be applied to the solution of the thin shear layer equations. The box method was introduced by Keller in 1970 [Ref. 4].

One of the basic ideas of the box method is to write the governing system of equations in the form of a first-order system. This system is solved by finite-difference approximations and Newton's method is applied to solve the equations. Finally, the resulting linear system is solved by the block-elimination method.

B. FALKNER-SKAN TRANSFORMATION

The thin shear layer equations for incompressible laminar flow take the form

$$\frac{\partial u}{\partial x} + \frac{\partial v}{\partial y} = 0 \quad (4.1)$$

$$u \frac{\partial u}{\partial x} + v \frac{\partial u}{\partial y} = - \frac{1}{\rho} \frac{dp}{dx} + \nu \frac{\partial^2 u}{\partial y^2} \quad (4.2)$$

Boundary conditions are prescribed at the surface

$$y = 0 \quad u = 0 \quad v = 0$$

and at the edge of the boundary layer

$$y \rightarrow \infty \quad u = U_e(x) \quad (4.3)$$

It is convenient to reformulate the equations using the streamfunction and the similarity concept. Therefore the Falkner-Skan transformation is introduced.

$$\eta = \left(\frac{U_e}{\nu x}\right)^{1/2} y = \frac{Re_x^{1/2}}{x} y \quad (4.4)$$

$$\psi(x, y) = (U_e \nu x)^{1/2} f(x, \eta) \quad (4.5)$$

Substituting Eqs. (4.4) and (4.5) into Eq. (4.2), we get the transformed momentum equation for 2-D laminar flows.

$$f''' + \frac{m+1}{2} f f'' + m[1 - (f')^2] = x \left(f' \frac{\partial f'}{\partial x} - f'' \frac{\partial f}{\partial x} \right) \quad (4.6)$$

where

$$m \equiv \frac{x}{U_e} \frac{dU_e}{dx}$$

(dimensionless pressure-gradient)

with the boundary conditions

$$\begin{aligned} \eta = 0 \quad f' = 0 \quad f = 0 \\ \eta = \eta_\infty \quad f' = 1 \end{aligned} \quad (4.7)$$

If f is a function of η only, the right-hand terms of Eq. (4.6) will be zero. Then this will be a third-order ordinary differential equation whose solution is well-known as a "similar flow." But, if f is a function of η and x (non-similar flows), we need a numerical procedure, such as the box method.

C. NUMERICAL FORMULATION (BOX METHOD)

First of all, the coordinates (x,y) of a given geometry must be transformed to coordinates (ξ,η) to apply the Box method (see Figure 4.1).

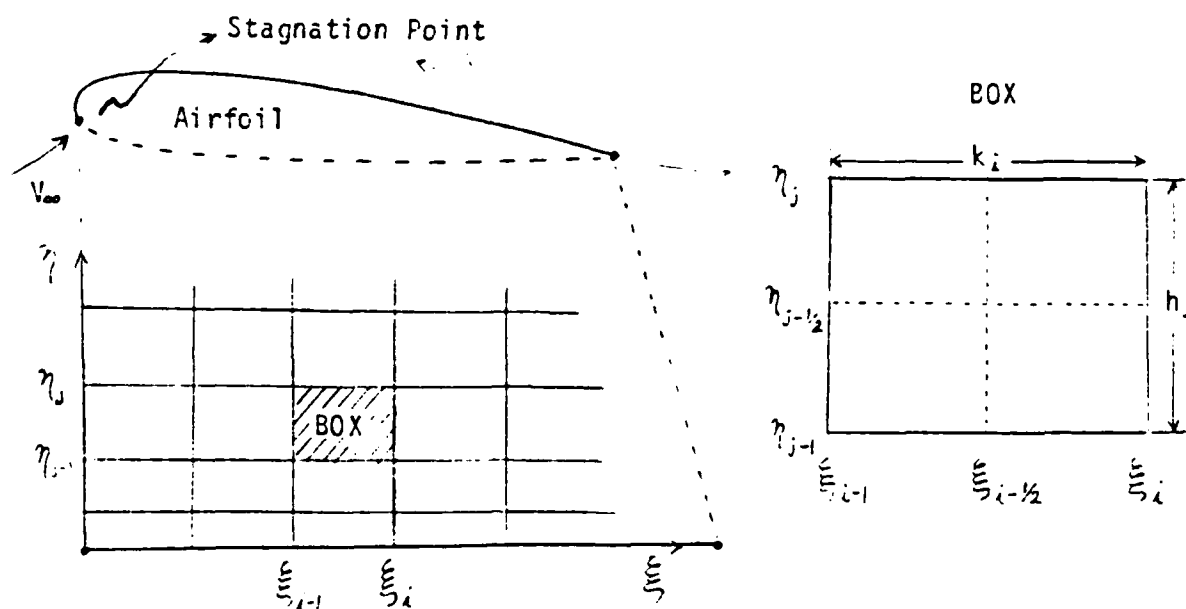


Figure 4.1. Transformed Coordinates of Upper Surface Airfoil and Net Rectangle for Difference Approximations

The boundary layer thickness in transformed coordinates is nearly independent of the streamwise distance and can be represented by a fixed number of profile points at fixed spacing.

One of the basic ideas of the Box method is to write the governing system of equations in the form of a first order system. We write Eq. (4.6) in terms of a first-order system of PDE's

$$f' = u(\xi, \eta) \quad (4.8a)$$

$$u' = v(\xi, \eta) \quad (4.8b)$$

$$(bv)' + \left(\frac{m+1}{2}\right)fv + m(1-u^2) = \xi \left(u \frac{\partial u}{\partial \xi} - v \frac{\partial f}{\partial \xi}\right) \quad (4.8c)$$

where a prime denotes differentiation with respect to η

$$\text{and} \quad b = 1 + v_t/v$$

with the boundary condition

$$f(\xi, 0) = 0, \quad u(\xi, 0) = 0, \quad u(\xi, \eta_\infty) = 1 \quad (4.9)$$

We denote the net points shown in Figure 4.1 as

$$\begin{aligned} \xi_0 &= 0 & \xi_i &= \xi_{i-1} + k_i & i &= 1, 2, \dots, I \\ \eta_0 &= 0 & \eta_j &= \eta_{j-1} + h_j & j &= 1, 2, \dots, J & \eta_J &= \eta_\infty \end{aligned}$$

And we can introduce the following approximations:

A) Coordinates of midpoints $(\xi_{i-\frac{1}{2}}, \eta_{j-\frac{1}{2}})$ and net functions
(g stands for f, u or v)

$$\xi_{i-\frac{1}{2}} \equiv \frac{1}{2}(\xi_i + \xi_{i-1}) \quad \eta_{j-\frac{1}{2}} \equiv \frac{1}{2}(\eta_j + \eta_{j-1}) \quad (4.10a)$$

$$g_j^{i-\frac{1}{2}} \equiv \frac{1}{2}(g_j^i + g_j^{i-1}) \quad g_{j-\frac{1}{2}}^i \equiv \frac{1}{2}(g_j^i + g_{j-1}^i) \quad (4.10b)$$

where $[]_j^i$ means the quantities (f or u or v) at point (ξ_i, η_j) .

B) Finite-difference approximation

From Eqs. (4.8a) and (4.8b), the centered-difference derivatives are

$$\frac{f_j^i - f_{j-1}^i}{h_j} = u_{j-\frac{1}{2}}^i \quad (4.11a)$$

$$\frac{u_j^i - u_{j-1}^i}{h_j} = v_{j-\frac{1}{2}}^i \quad (4.11b)$$

After introducing these approximations into Eq. (4.8) and rearranging (the known quantities are moved to the right hand side), we get the equation (4.12c) which is centered about the point $(\xi_{i-\frac{1}{2}}, \eta_{j-\frac{1}{2}})$. This represents the relationship of quantities between the points of the box.

$$f_j^i - f_{j-1}^i - \frac{h_j}{2}(u_j^i + u_{j-1}^i) = 0 \quad (4.12a)$$

$$u_j^i - u_{j-1}^i - \frac{h_j}{2}(v_j^i + v_{j-1}^i) = 0 \quad (4.12b)$$

$$\begin{aligned} (b_j^i v_j^i - b_{j-1}^i v_{j-1}^i)/h_j + \alpha_1 (fv)_{j-\frac{1}{2}}^i - \alpha_2 (u^2)_{j-\frac{1}{2}}^i \\ + \alpha (v_{j-\frac{1}{2}}^{i-1} f_{j-\frac{1}{2}}^i - f_{j-\frac{1}{2}}^{i-1} v_{j-\frac{1}{2}}^i) = R_{j-\frac{1}{2}}^{i-1} \end{aligned} \quad (4.12c)$$

where

$$\alpha = \frac{\xi_{i-\frac{1}{2}}}{i}, \quad \alpha_1 = \frac{m_i+1}{2} + \alpha, \quad \alpha_2 = m_i + \alpha$$

$$R_{j-\frac{1}{2}}^{i-1} = \{-L_{j-\frac{1}{2}} + \alpha[(fv)_{j-\frac{1}{2}}^{i-1} - (u^2)_{j-\frac{1}{2}}^{i-1}]\}^{i-1} - m_i^i$$

$$L_{j-\frac{1}{2}}^{i-1} = \left\{ \frac{b_j^i v_j^i - b_{j-1}^i v_{j-1}^i}{h_j} + \frac{m_i+1}{2} (fv)_{j-\frac{1}{2}}^{i-1} + m_i [1 - (u^2)_{j-\frac{1}{2}}^{i-1}] \right\}^{i-1}$$

The last of the above equations is non-linear. Therefore we introduce Newton's method to solve this system. We set

$$g_j^{(n+1)} = g_j^{(n)} + \delta g_j^{(n)} \quad n = 0, 1, 2, \dots \quad (4.13)$$

where the superscript in parentheses is the iteration counter with initial condition

$$\begin{aligned}
f_0^{(0)} &= 0 & u_0^{(0)} &= 0 & v_0^{(0)} &= v_0^{i-1} \\
f_j^{(0)} &= f_j^{i-1} & u_j^{(0)} &= u_j^{i-1} & v_j^{(0)} &= v_j^{i-1} \\
f_J^{(0)} &= f_J^{i-1} & u_J^{(0)} &= 1 & v_J^{(0)} &= v_J^{i-1}
\end{aligned} \tag{4.14}$$

$$1 \leq j \leq J-1$$

Introducing Eq. (4.13) to Eq. (4.12) and dropping the quadratic terms in g_i , we get (superscripts i and n are dropped for simplicity)

$$\delta f_j - \delta f_{j-1} - \frac{h_j}{2}(\delta u_j + \delta u_{j-1}) = (r_1)_j \tag{4.15a}$$

$$\delta u_j - \delta u_{j-1} - \frac{h_j}{2}(\delta v_j + \delta v_{j-1}) = (r_3)_{j-1} \tag{4.15b}$$

$$\begin{aligned}
&(S_1)_j \delta v_j + (S_2)_j \delta v_{j-1} + (S_3)_j \delta f_j + (S_4)_j \delta f_{j-1} \\
&+ (S_5)_j \delta u_j + (S_6)_j \delta u_{j-1} = (r_2)_j
\end{aligned} \tag{4.15c}$$

where all terms are explained in Reference 5, with the boundary conditions

$$\delta f_0 = 0 \quad \delta u_0 = 0 \quad \delta u_J = 0 \tag{4.16}$$

D. BLOCK ELIMINATION METHOD

This is a very effective way to solve linear difference equations, discussed by Keller in 1974 [Ref. 6]. We write

Eq. (4.15) in a matrix-vector form

$$\Lambda \delta = r \quad (4.17)$$

where

$$\Lambda \equiv \begin{bmatrix} A_0 & C_0 & & \\ B_1 & A_1 & C_1 & \\ & \ddots & \ddots & \ddots \\ & & B_{J-1} & A_{J-1} & C_{J-1} \\ & & & B_J & A_J \end{bmatrix} \quad \delta \equiv \begin{bmatrix} \delta_0 \\ \delta_1 \\ \vdots \\ \delta_J \end{bmatrix} \quad r \equiv \begin{bmatrix} r_0 \\ r_1 \\ \vdots \\ r_J \end{bmatrix}$$

where

$$\begin{aligned} A_0 &= \begin{bmatrix} 1 & 0 & 0 \\ 0 & 1 & 0 \\ 0 & -1 & -h_1/2 \end{bmatrix} & A_J &= \begin{bmatrix} 1 & -h_J/2 & 0 \\ (S_3)_J & (S_5)_J & (S_1)_J \\ 0 & 1 & 0 \end{bmatrix} \\ A_j &= \begin{bmatrix} 1 & -h_j/2 & 0 \\ (S_3)_j & (S_5)_j & (S_1)_j \\ 0 & -1 & -h_{j+1}/2 \end{bmatrix} & C_j &= \begin{bmatrix} 0 & 0 & 0 \\ 0 & 0 & 0 \\ 0 & 1 & -h_{j+1}/2 \end{bmatrix} & 1 \leq j \leq J-1 \\ B_j &= \begin{bmatrix} -1 & -h_j/2 & 0 \\ (S_4)_j & (S_6)_j & (S_2)_j \\ 0 & 0 & 0 \end{bmatrix} & & 1 \leq j \leq J \end{aligned}$$

where

$$\delta_j \equiv \begin{bmatrix} \delta f_j \\ \delta u_j \\ \delta v_j \end{bmatrix} \quad 0 \leq j \leq J$$

$$r_j = \begin{bmatrix} (r_1)_j \\ (r_2)_j \\ (r_3)_j \end{bmatrix} \quad 1 \leq j \leq J-1 \quad r_0 = \begin{bmatrix} 0 \\ 0 \\ (r_3)_0 \end{bmatrix}$$

$$r_J = \begin{bmatrix} (r_1)_J \\ (r_2)_J \\ 0 \end{bmatrix}$$

According to Keller's block elimination method, we have to factorize the matrix Λ .

$$\Lambda = P \times Q \quad (4.18)$$

where

$$P \equiv \begin{bmatrix} I & & & \\ & P_1 & I & \\ & & \ddots & \\ & & & P_J & I \end{bmatrix} \quad Q \equiv \begin{bmatrix} Q_0 & C_0 & & \\ & Q_1 & C_1 & \\ & & \ddots & \\ & & & Q_J & C_{J-1} \end{bmatrix}$$

I is the identity matrix

$$I = \begin{pmatrix} 1 & 0 & 0 \\ 0 & 1 & 0 \\ 0 & 0 & 1 \end{pmatrix}$$

From Eq. (4.18), we find that

$$Q_0 = A_0 \quad (4.19a)$$

$$P_j Q_{j-1} = B_j \quad j = 1, 2, \dots, J \quad (4.19b)$$

$$Q_j = A_j - P_j C_{j-1} \quad j = 1, 2, \dots, J \quad (4.19c)$$

Keller showed that the matrix P_j has the same structure as the matrix B_j . From Eq. (4.19), we derive the elements of P_j and Q_j .

$$P_j = \begin{pmatrix} (p_{11})_j & (p_{12})_j & (p_{13})_j \\ (p_{21})_j & (p_{22})_j & (p_{23})_j \\ 0 & 0 & 0 \end{pmatrix}$$

$$Q_j = \begin{pmatrix} (q_{11})_j & (q_{12})_j & (q_{13})_j \\ (q_{21})_j & (q_{22})_j & (q_{23})_j \\ 0 & -1 & -h_{j+1}/2 \end{pmatrix} \quad 0 \leq j \leq J-1$$

Each element of P_j and Q_j is explained in Reference 5. If we let

$$Q\delta = W \quad (4.20)$$

Introducing Eqs. (4.20) and (4.18) into Eq. (4.17),

$$PW = r \quad (4.21)$$

Then, from Eq. (4.21), we find that

$$W_0 = r_0$$

$$W_j = r_j - P_j W_{j-1} \quad 1 \leq j \leq J$$

The elements of W_j are listed in Reference 5. Finally, we get the matrix form to get δ from Eq. (4.20).

$$\begin{bmatrix} Q_0 & C_0 & & & \\ & Q_1 & \ddots & & \\ & & \ddots & C_{J-1} & \\ & & & Q_{J-1} & \\ & & & & Q_J \end{bmatrix} \begin{bmatrix} \delta_0 \\ \delta_1 \\ \vdots \\ \delta_J \end{bmatrix} = \begin{bmatrix} W_0 \\ W_1 \\ \vdots \\ W_J \end{bmatrix} \quad (4.22)$$

From Eq. (4.22), we find that

$$Q_J \delta_J = W_J \quad (4.23a)$$

$$Q_j \delta_j = W_j - C_j \delta_{j+1} \quad j = J-1, J-2, \dots, 0 \quad (4.23b)$$

Therefore δ_j can be obtained by calculating the terms Q_j , C_j and W_j (see Reference 5).

V. INTERACTION METHOD

A. INTRODUCTION

Interactive methods provide a special coupling between viscous and inviscid flows. They are intended to compute flows including separation. Thus these methods may be regarded as an alternative to the Navier-Stokes solvers, which are hardly engineering tools because of their huge computer time and storage requirements.

The classical method to compute viscous flows past airfoils proceeds as follows: The velocity distribution is computed by any appropriate inviscid flow solver. The output of the inviscid flow solver becomes the input of the viscous flow solver. Solving for viscous flow consists of integrating the boundary layer equations. Provided that the flow remains attached this procedure allows a reliable prediction of lift and drag. Information is transferred only once from inviscid to viscous regions. However, many flows cannot be modelled by one-time information transfers.

Separation bubbles and separated flows especially require a close coupling between viscous and inviscid regions. Interaction schemes provide a better exchange of information between these two regions.

The elements of interaction schemes are: direct or inverse inviscid flow solver and direct or inverse viscous flow solver.

Boundary Condition Flow	Direct	Inverse
Inviscid	<ul style="list-style-type: none"> • Zero normal velocity at the surface 	<ul style="list-style-type: none"> • Prescription of velocity distribution
Viscous	<ul style="list-style-type: none"> • No slip condition • Prescription of external velocity 	<ul style="list-style-type: none"> • No slip condition • Prescription of displacement thickness

The direct boundary layer method has the disadvantage that the boundary layer equations are singular at the point of separation. However, if the external velocity is computed by prescribing a displacement thickness (known as the inverse boundary layer method), they can be integrated through the point of separation.

The next problem associated with the regions of reversed flow is numerical instability, because downstream marching procedures cannot be applied in regions of reversed flow. The most common approximation to get this instability under control, the so-called FLARE approximation, neglects the momentum transport term $u \partial u / \partial x$ in regions of reversed flow as long as this region is small. However, as the size of this region increases, the FLARE approximation becomes inaccurate. One of the procedures which can be taken into account is called the DUIT (Downstream, Upstream Iteration). It consists of a sequence of alternating up and downstream sweeps.

There are several types of recently developed interaction models. All procedures have to solve both the inviscid (Laplace

equation) and viscous flow, whose equations can be written according to

$$\frac{\partial u}{\partial x} + \frac{\partial v}{\partial y} = 0 \quad (5.1)$$

$$u \frac{\partial u}{\partial x} + v \frac{\partial u}{\partial y} = U_e \frac{dU_e}{dx} + \frac{\partial}{\partial y} (b v \frac{\partial u}{\partial y}) \quad (5.2)$$

where

$b = 1 = \text{constant}$ in laminar flow

$b = 1 + v_t/\nu$ in turbulent flow

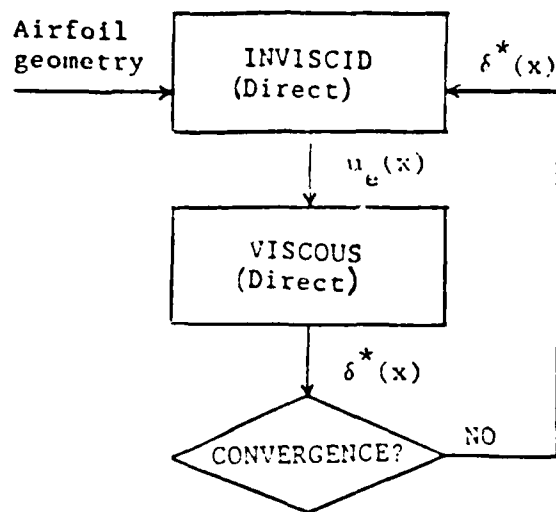
Four interaction models can be distinguished: Direct, Inverse, Semi-inverse, and Simultaneous interaction methods which are subject to different boundary conditions.

The most advanced interaction scheme is the simultaneous interaction. We call it the "strong interaction" (direct and inverse interactions guarantee weak coupling only). Examples in Section V.D are computed by the Cebeci program using this method. Good agreement is obtained between the results of interaction schemes and experimental results.

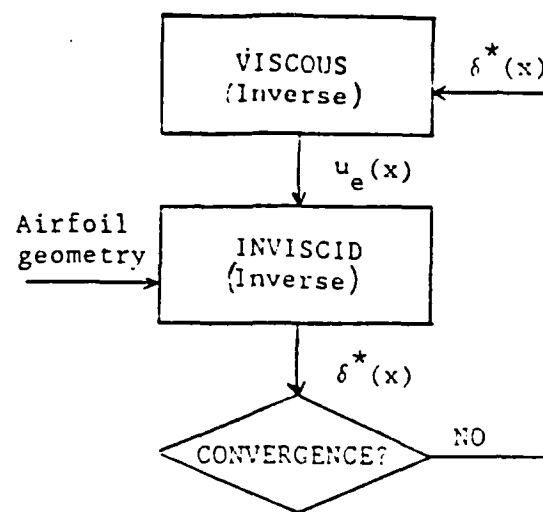
B. FOUNDATION OF THE INTERACTION SCHEMES

1. Direct Interaction Scheme

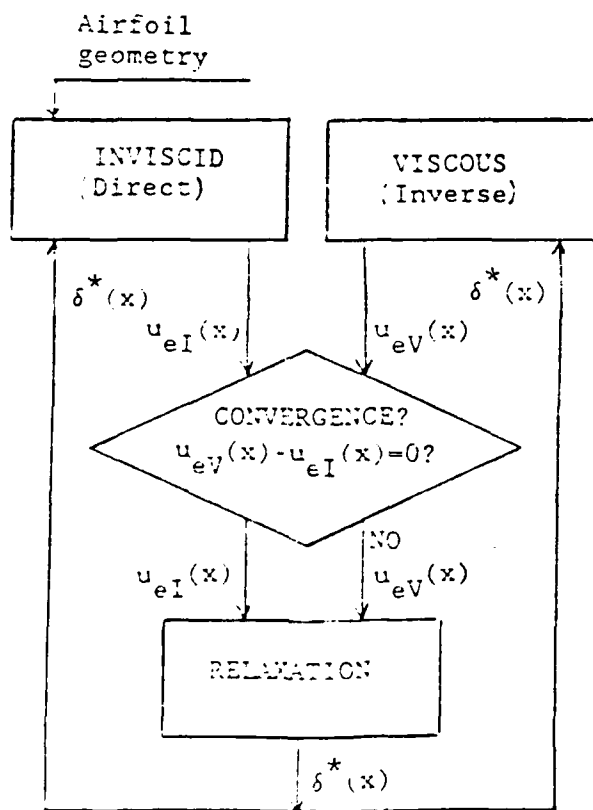
The direct interaction model is composed of a direct inviscid and a direct viscous flow solver (see Figure 5.1a). The usual sequence is:



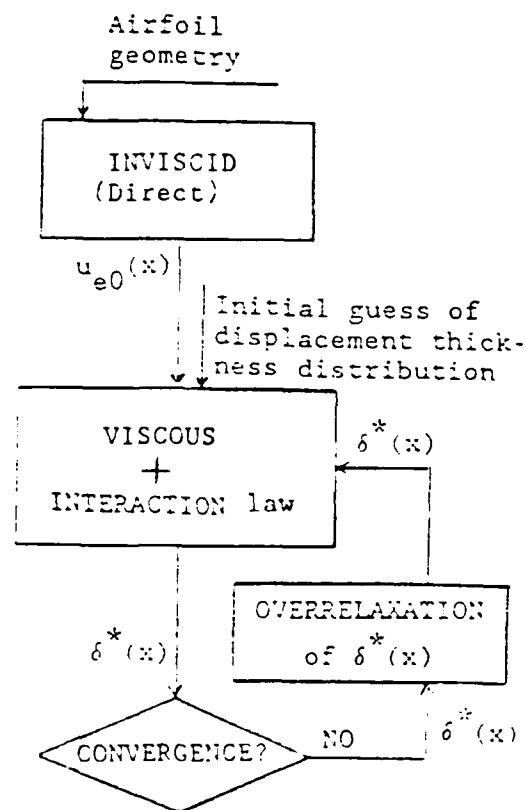
a) DIRECT



b) INVERSE



c) SEMI-INVERSE



d) SIMULTANEOUS

Figure 5.1. Global Organization of Interaction Methods

- (1) Calculate the external velocity distribution by inviscid flow computations.
- (2) Calculate the displacement thickness, δ^* , by viscous flow computations using the external velocity as boundary condition.
- (3) Compute an updated shape of the displacement body and repeat steps 1 and 2 until the results converge.

Unfortunately, the direct boundary layer method suffers numerical breakdown at the point of separation (Goldstein singularity). Therefore this scheme is not appropriate to handle airfoil flows with separation.

2. Inverse Interaction Scheme

This method was introduced to overcome the singularity problems near separation. It combines an inverse inviscid and an inverse viscous flow solver (see Figure 5.1b). However, the overall procedure suffers from very slow convergence. Due to this shortcoming one shall apply this inverse scheme to regions of separated flow only.

3. Semi-Inverse Interaction Scheme

This method combines a direct inviscid flow solver with an inverse viscous flow solver with the same input (displacement thickness). This leads to two external velocity distributions, $U_{eI}(x)$ and $U_{eV}(x)$ (see Figure 5.1c). Satisfactory convergence is ensured by a relaxation formula, which is introduced to define an updated displacement thickness distribution.

$$\delta_{new}^*(x) = \delta_{old}^*(x) [1 + \omega \left(\frac{U_{eV}(x)}{U_{eI}(x)} - 1 \right)] \quad (5.3)$$

where ω is a relaxation parameter. The numerical weakness of the purely inverse scheme is improved by this method, but both inviscid and viscous regions are still coupled loosely.

4. Simultaneous Interaction Scheme

The simultaneous interaction scheme emphasizes strong interaction between the outer inviscid and the inner viscous region. The external velocity $U_e(x)$ and the displacement thickness $\delta^*(x)$ are treated as unknown quantities. An additional relation is added, the so-called interaction law which can be given by the "blowing velocity" concept.

The equations are solved by the inverse method with successive sweeps over the airfoil surface (see Figure 5.1d). This method is compatible with the weak interaction scheme where both inviscid and viscous regions are coupled loosely.

For each sweep, the external velocity for the boundary layer equation is written as

$$U_e(x) = U_e^0(x) + \delta U_e(x) \quad (5.4)$$

where

$U_e^0(x)$ is the inviscid velocity;

$\delta U_e(x)$ is the perturbation due to the displacement effect of a boundary layer.

The blowing velocity concept is introduced to get the perturbation velocity δU_e by the interaction law. The displacement

effect of a boundary layer can be modelled by ejecting fluid at the airfoil's surface (see Figure 5.2).

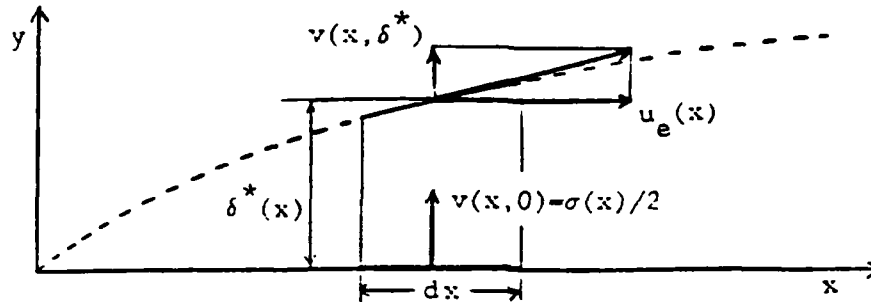


Figure 5.2. Blowing Velocity Concept

A properly arranged source distribution on the surface displaces the streamlines away from the surface such that the virtual displacement body becomes a streamline.

Our first goal is to determine the source strengths such that the tangential flow condition on the displacement body takes the form

$$\frac{v(x, \delta^*)}{U_e(x)} = \frac{d\delta^*}{dx} \quad (5.5)$$

To achieve this goal we use the thin airfoil approximation:

- (1) The displacement thickness is assumed to be so small that u -velocity components do not vary across the layer.
- (2) The airfoil in this connection can be represented by a straight line. This approximation implies that the blowing velocity $v(x, 0)$ equals half of the source strength.

Therefore, .

$$\begin{aligned}
 \frac{\sigma(x)}{2} &= v(x, 0) \\
 &= v(x, \delta^*) - \int_0^{\delta^*} \frac{\partial v}{\partial y} dy \\
 &= U_e \frac{d\delta^*}{dx} + \frac{dU_e}{dx} \delta^* \\
 &= \frac{d}{dx}(U_e \delta^*) \tag{5.6}
 \end{aligned}$$

where $\frac{d}{dx}(U_e \delta^*)$ is defined as blowing velocity. Our second goal is to relate the perturbation velocity, δU_e to the blowing velocity. This process is quite similar to evaluating tangential velocities in the panel method. In fact, this is even simpler because of the straight line surface.

$$\delta U_e = \frac{1}{2\pi} \int_{x_a}^{x_b} \frac{\sigma(\xi)}{x - \xi} d\xi \tag{5.7}$$

where the interaction region is limited to a finite range $x_a \leq x \leq x_b$. This integral is referred to as the Hilbert integral. Rewriting Eq. (5.4), we finally obtain the interaction law.

$$U_e(x) = U_e^0(x) + \frac{1}{\pi} \int_{x_a}^{x_b} \frac{d}{d\xi}(U_e \delta^*) \frac{d\xi}{x - \xi} \tag{5.8}$$

The numerical implementation of Eq. (5.8) requires a discrete approximation of the Hilbert integral. This can be performed by using the trapezoidal rule.

The examples in Section V.D demonstrate that this interaction method can give reliable results for flows up to high angle of attack, including flows with bubbles and separation.

C. CONSIDERATION OF BOUNDARY LAYER TRANSITION AND OF TURBULENT FLOW MODELLING

1. Transition

One of the most important parameters to predict the drag and lift of an airfoil is the transition point. Boundary layer transition is affected by many parameters, for example, the pressure distribution (major parameter), the wall roughness and the intensity of the free stream turbulence, etc. Because of this fact, the theoretical modeling of transition is very complicated and one therefore resorts to experimental information.

In the Cebeci program, the following experimental correlation formula is used, which was given by Cebeci and Smith (1974) as a relation between R_θ and Re_x at transition.

$$R_{\theta_{tr}} = 1.174 \left(1 + \frac{22400}{Re_{x_{tr}}} \right) Re_{x_{tr}}^{0.46} \quad (5.9)$$

where

$$Re_x \equiv U_e x / \nu$$

$$R_\theta \equiv U_e \theta / \nu$$

and θ is the momentum thickness.

2. Turbulent Flow Model

Unlike laminar flows, turbulent flows have a complicated time-dependent behavior. It is too difficult to deal with the instantaneous properties. Thus, the mean-flow properties are applied in turbulent flow.

The most common mean-flow models are the "eddy-viscosity" formula which are based on thin shear layer assumptions.

$$-\rho \overline{u'v'} = \rho \nu_t \frac{\partial u}{\partial y} \quad (5.10)$$

where ν_t is related empirically to the mean flow velocity gradient and the length scale. In the Cebeci program, ν_t is presented by the algebraic eddy-viscosity formulation of Cebeci and Smith.

$$\nu_t = \begin{cases} \{0.4y[1-\exp(-y/A)]\}^2 \left| \frac{\partial u}{\partial y} \right| \gamma_{tr} & 0 \leq y \leq y_c \\ \alpha \left| \int_0^\infty (U_e - u) dy \right| \gamma_{tr} & y_c \leq y \leq \delta \end{cases} \quad (5.11)$$

More detailed descriptions are listed in Reference 7.

D. EXAMPLES

The subsequent examples were computed using a program developed by Cebeci and coworkers [Ref. 17], on the NPS IBM 370.

1. Demonstration of the Program Capabilities

The velocity profiles on both upper and lower surfaces, as well as in the wake, are presented in Figure 5.3. At this angle of attack ($\alpha = 10^\circ$), transition occurs very close to the leading edge on the upper surface. The boundary layer thickness is quite thin in the accelerated flow region (right after the leading edge), but it grows thicker farther downstream in the decelerated flow region (near the trailing edge). Eventually, we find a small reversed flow region just before the trailing edge in this case. The wake region shows the mixing layer which decays with increasing downstream distance.

Figure 5.4 demonstrates how lift, drag and the location of transition depend on the angle of attack. The skin friction drag is dominant at low angles of attack, the pressure drag at high angles of attack (see Figure 5.4b).

Figure 5.5 shows the distributions of the skin friction coefficient, displacement thickness and shape parameter in dependence of Reynolds number and angle of attack. In the attached flow, the skin friction coefficient decreases along the downstream direction until the point of transition (laminar region), but increases steeply after transition and then decreases again because the skin friction is related to the slope of the velocity profile, $\partial u / \partial y$, at the surface. At high angles of attack, transition on the upper surface occurs close to the leading edge and the negative skin friction coefficient near the trailing edge indicates separated flow.

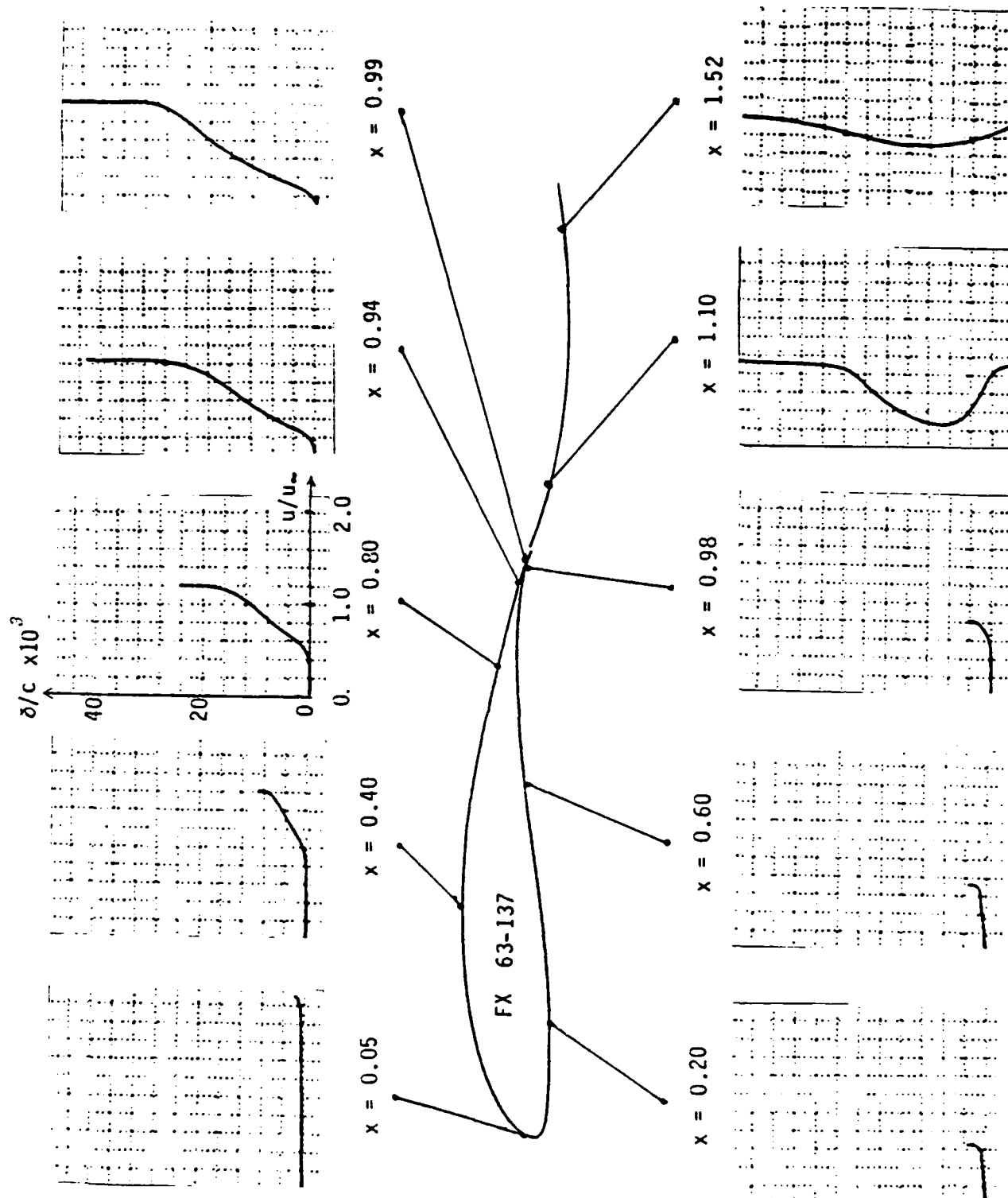


Figure 5.3. Velocity Profiles on the Surface and Wake of FX 63-137 Airfoil ($\alpha = 10^\circ$, $Re = 5 \times 10^6$)

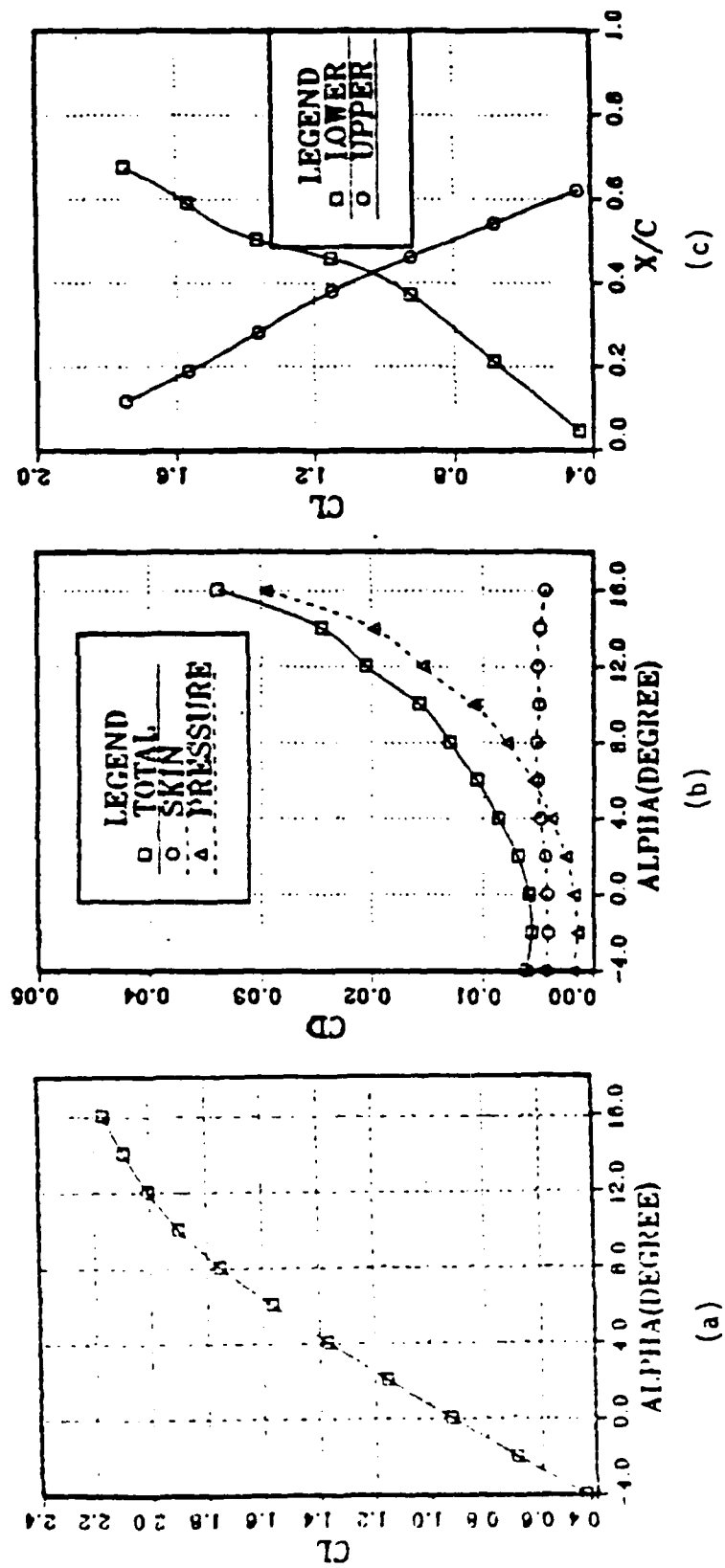
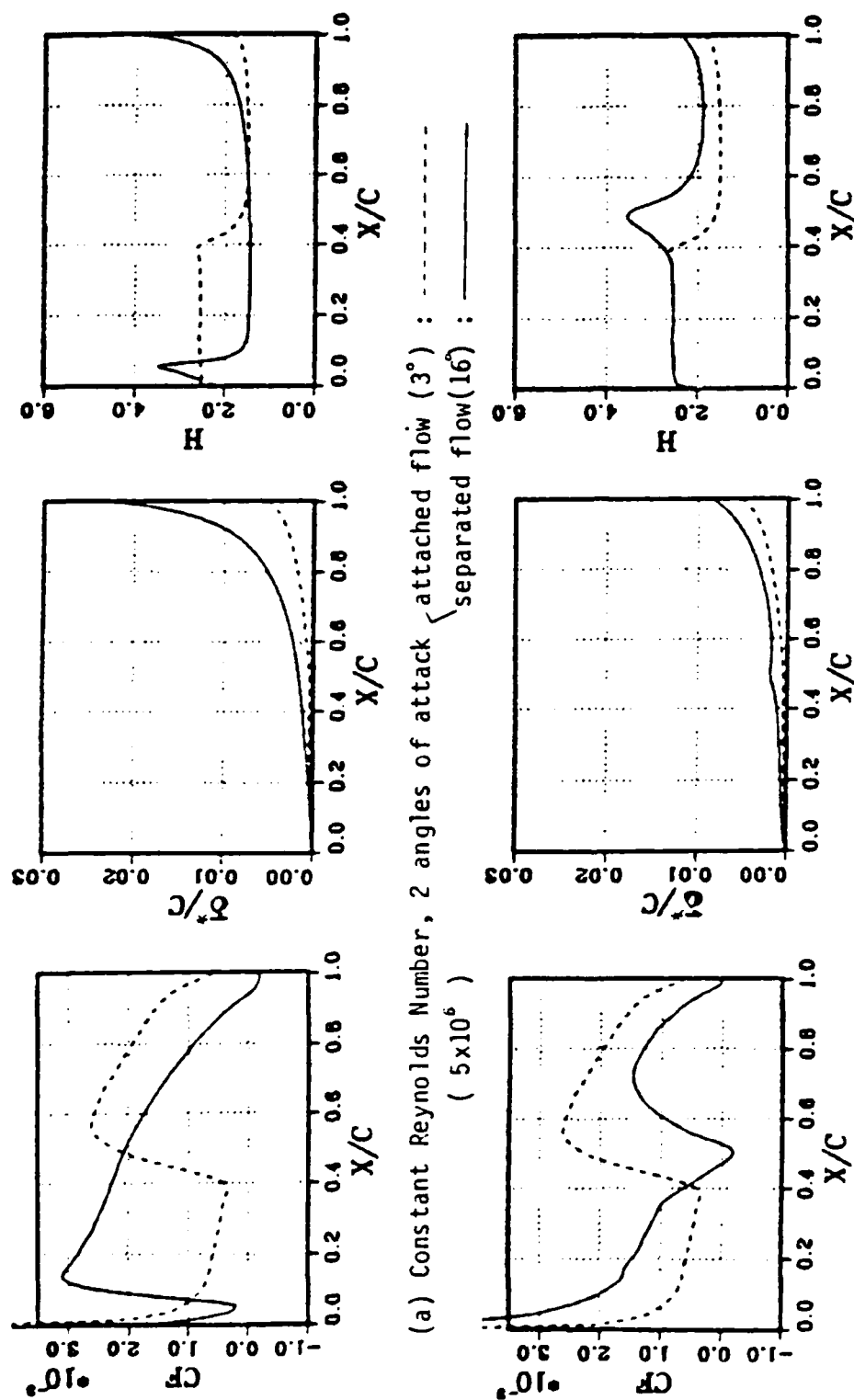


Figure 5.4. (a) Lift, (b) Drag, (c) Transition Points
Calculations (FX 63-137 Airfoil, $Re = 5 \times 10^6$)



(a) Constant Reynolds Number, 2 angles of attack $\left(3^\circ \right)$: $---$ attached flow (5×10^6)
 $---$ separated flow (16°) : $---$ a short bubble ($.8 \times 10^6$) : $---$

(b) Constant angle of attack, 2 Reynolds Number $\left(3^\circ \right)$: $---$ attached flow (5×10^6)
 $---$ a short bubble ($.8 \times 10^6$) : $---$

Figure 5.5. Skin Friction Coefficient, Displacement

Thickness and Shape Parameter for FX 63-137

Also the displacement thickness and the shape parameter increase drastically in regions of separated flow (see Figure 5.5a).

At low Reynolds numbers, laminar flow can separate at mid-chord and reattach (we call this phenomenon a "bubble"). Reattachment can often occur if the pressure gradient decreases rapidly soon after separation, so that a strong reversed flow is not established. Thus the shear layer reattaches onto the surface. Accordingly, the displacement thickness and the shape parameter increase in the bubble region (see Figure 5.5b).

2. Comparison with Experimental Results

The comparison of pressure distributions is shown in Figure 5.6. The overall lift of inviscid calculations deviates 20% from the experimental results. The interaction method improves the accuracy, but the computation still overestimates the lift. The lift coefficient obtained by Cebeci's program is approximately 10% larger than the measured one (see Reference 8).

Figure 5.7 demonstrates that the accuracy of this method drops with lower Reynolds numbers. The reasons for this decreased accuracy at low Reynolds numbers are the higher probability to separate and the used turbulence model, which seems to be inappropriate for low Reynolds numbers. Therefore, low Reynolds numbers and high angles of attack pose severe limitations (see Figure 5.7a & b). The experimental results are taken from References 7 and 9.

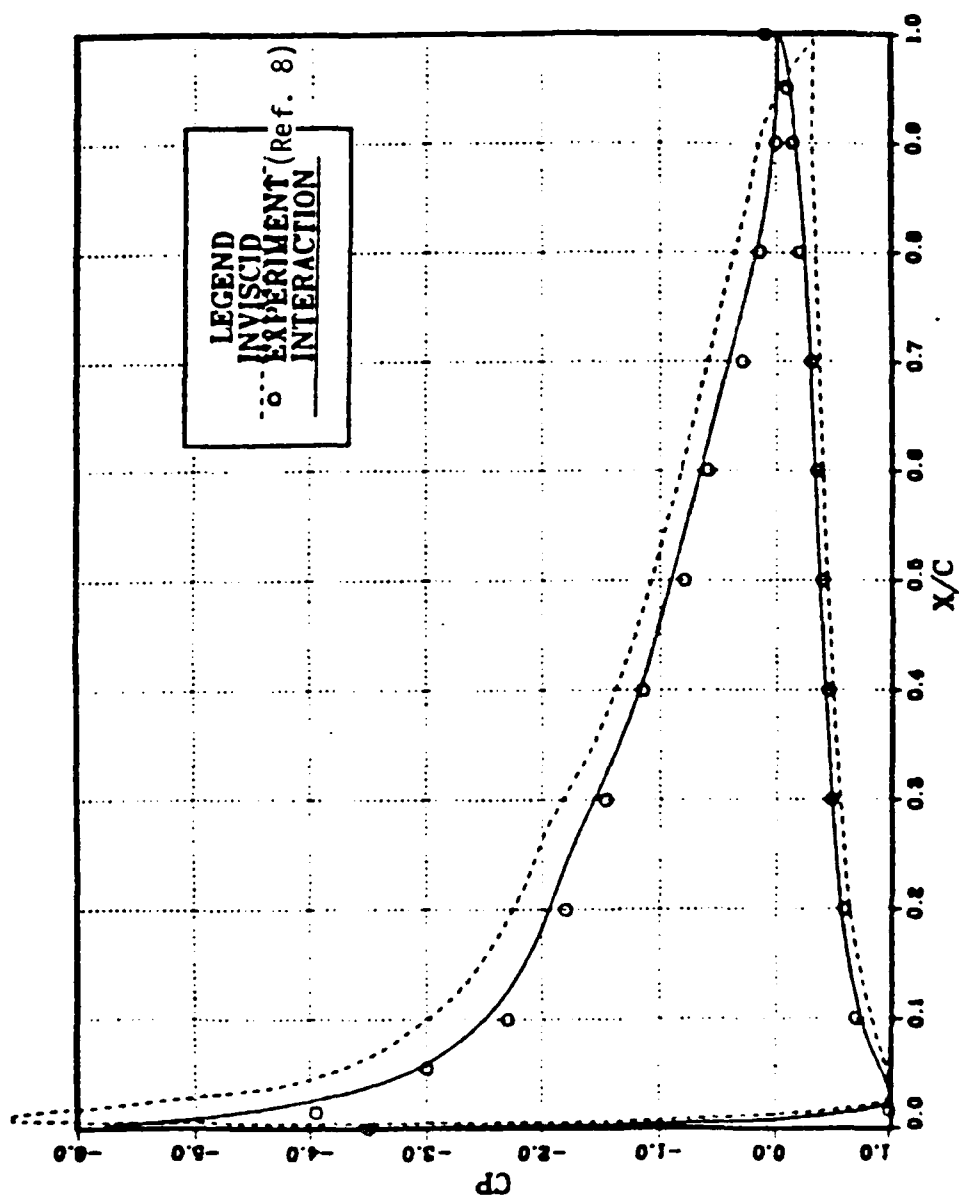


Figure 5.6. Comparison of Pressure Distributions (NACA 4412 Airfoil, $\alpha = 12.15^\circ$)

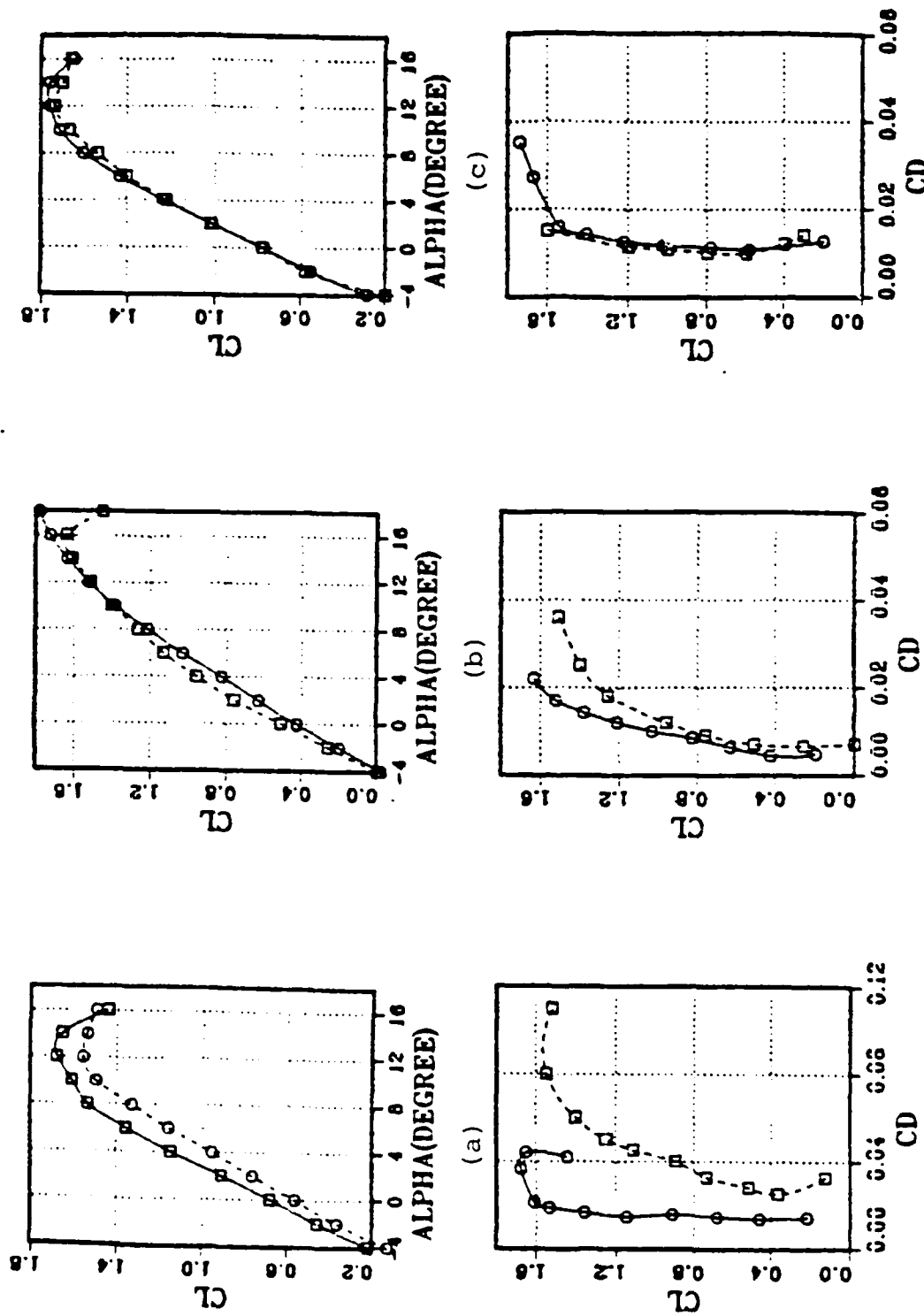


Figure 5.7 C_l and C_d Curves for (a) FX 63-137, $Re = 199487$
 (b) GA-1, $Re = 1900000$, (c) FX 63-137, $Re = 280000$
 (Source of experimental results: (a)Ref.9 (b)Ref.7 (c)Ref.10)

AD-A168 481

CONTRIBUTION TO THE ANALYSIS OF HIGH-LIFT AIRFOIL
AERODYNAMICS(U) NAVAL POSTGRADUATE SCHOOL MONTEREY CA
H W LEE MAR 86

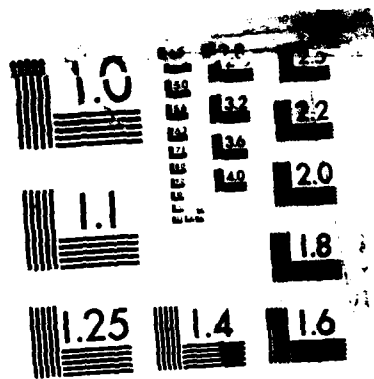
2/2

UNCLASSIFIED

F/G 28/4

NL

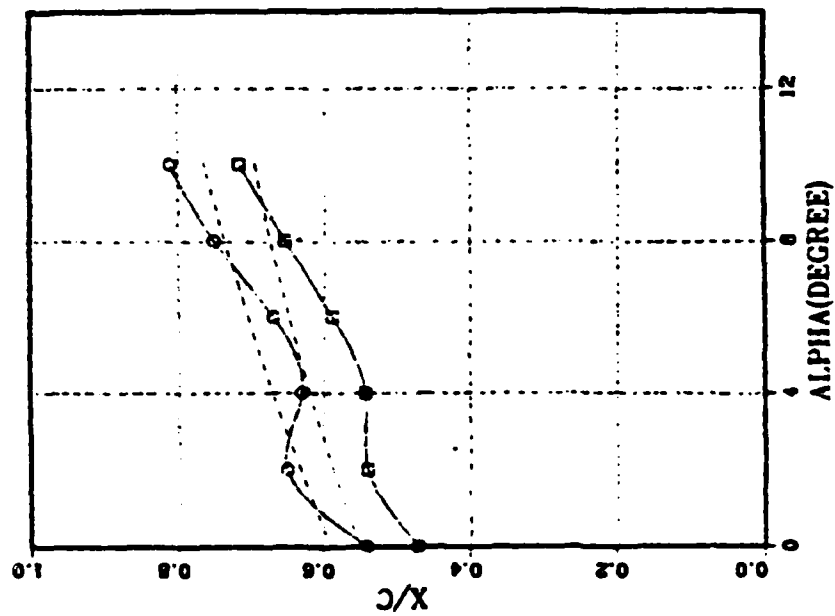




MICROCOPY RESOLUTION TEST CHART
NATIONAL BUREAU OF STANDARDS-1963-A

On the other hand, experimental measurements should not be expected to be exact. Turbulence level and interference effects influence the wind tunnel measurements. Figure 5.7c shows good agreement between computed and experimental results taken from Reference 10, at low Reynolds numbers.

The location of transition and separation points have an important influence on the lift and drag coefficients. Figure 5.8 shows that the prediction of laminar separation, reattachment, transition and separation points on the airfoil surfaces are in reasonable agreement with the experimental data taken from Reference 9.



--- : Experimental (Ref. 18)
 — : Interaction method

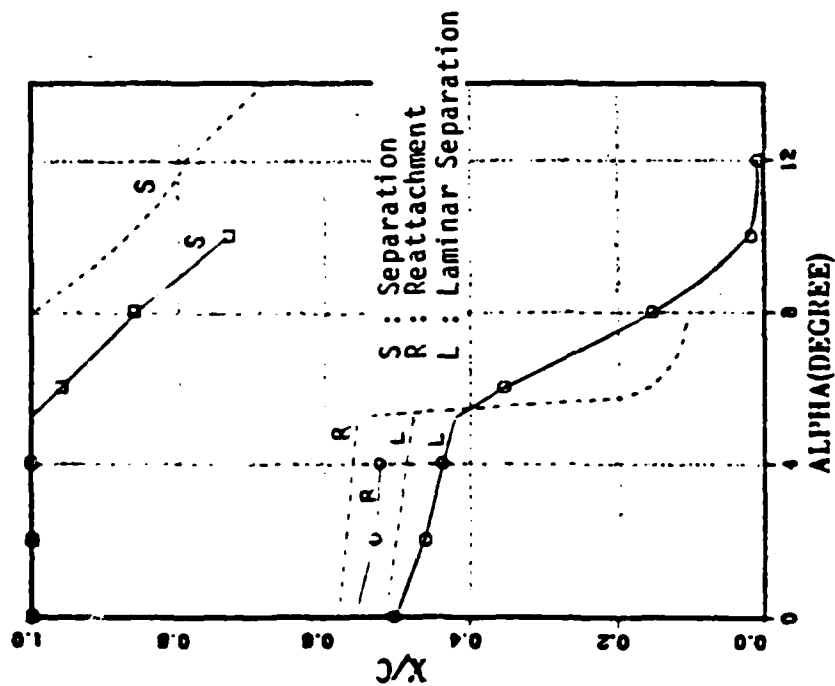


Figure 5.8. Transition and Separation Positions for NACA 64₃-418,
 $Re = 0.93 \times 10^6$

VI. SUMMARY AND RECOMMENDATIONS

This thesis treats the problem of incompressible two-dimensional steady flow past airfoils or airfoil combinations at large angles of attack. A panel method was developed to compute the inviscid flow over two cylinders, airfoil-flap combinations and airfoils in ground effect. In addition, Cebeci's viscous/inviscid interaction method was applied to several airfoils and compared with available experimental data. The agreement is generally quite encouraging. The calculations show the sensitivity of the computations to Reynolds number and transition. More work is required to evaluate the potential and limitations of the viscous/inviscid interaction method.

LIST OF REFERENCES

1. Smith, A.M.O., and Hess, J.L., "Calculation of Potential Flow About Arbitrary Bodies." In Kuchemann, Progress in Aeronautical Sciences, Vol. 8, 1967.
2. Martenson, E., "The Calculation of Pressure Distribution on a Cascade of Thick Airfoils by Means of Fredholm Integral Equations of the Second Kind," NASA TT F-702, 1971.
3. Davenport, F.J., "Singularity Solutions to General Potential Flow Airfoil Problems," D6-7202, Boeing Airplane Company, 1963.
4. Keller, H.B., Numerical Solutions of Partial Differential Equations, Vol. II, Academic Press, New York, 1970.
5. Cebeci, Tuncer and Bradshaw, Peter, Momentum Transfer in Boundary Layers, McGraw-Hill Book Company, 1977.
6. Keller, H.B., "Accurate Difference Methods for Nonlinear Two-Point Boundary-Value Problems," SIAM J. Numer. Anal., Vol. 11, 1974.
7. McGhee, R.J., and Beasley, W.D., "Low-Speed Aerodynamic Characteristics of a 17-Percent-Thick Airfoil Section Designed for General Aviation Applications," NASA TN D-7428, 1973.
8. Hastings, R.C., and Williams, B.R., "Studies of the Flow Filled Near an NACA 4412 Aerofoil at Nearly Maximum Lift," in 3rd Symposium on Numerical and Physical Aspects of Aerodynamic Flows, 1985.
9. Mueller, T.J., "Low Reynolds Number Vehicles," AGARD Graph No. 288, 1985.
10. Althaus/Wortmann, Stuttgarter Profilkatalog I, Vieweg, 1979.
11. Schlichting, H., Boundary-Layer Theory, McGraw-Hill Book Company, New York, 1968.
12. Gostelow, J.P., Cascade Aerodynamics, Pergamon Press, 1984.
13. Cebeci, Tuncer, Numerical and Physical Aspects of Aerodynamic Flows, Springer-Verlag, 1982.

14. Kuethe, Arnold M., and Chow, Chuen-Yen, Foundations of Aerodynamics, Wiley, 1976.
15. Cebeci, Tuncer, "Finite-Difference Solution of Boundary Layer Flows with Separation," California State University, Long Beach, Report ME-84-4, 1984.
16. Abbott and Doenhoff, Theory of Wing Sections, Dover Publications, Inc., 1958.
17. Cebeci, T. (Private Communication).
18. Render, P.M., Stollery, J.L., and Williams, B.R., "Aerofoils at Low Reynolds Numbers - Prediction and Experiment", in 3rd Symposium on Numerical and Physical Aspects of Aerodynamic Flows, 1985.

INITIAL DISTRIBUTION LIST

	No. Copies
1. Defense Technical Information Center Cameron Station Alexandria, Virginia 22304-6145	2
2. Library, Code 0142 Naval Postgraduate School Monterey, California 93943-5002	2
3. Chairman, Dept. of Aeronautics, Code 67 Naval Postgraduate School Monterey, California 93943-5000	10
4. Personnel Management Office Air Force Headquarters Dae-Bang Dong Dong-jak Ku Seoul, KOREA	2
5. Lee, Hee Woo 62-54 Jangwi-2 Dong Sung buk-Ku Seoul, KOREA	10
6. Paik, Seung Wook SMC #2675 Naval Postgraduate School Monterey, California 93943-5000	1

END
DTIC

7-86